
BONSAI: Bayesian Optimization with Natural Simplicity and Interpretability

Samuel Daulton*
Meta

David Eriksson
Meta

Maximilian Balandat
Meta

Eytan Bakshy
Meta

Abstract

Bayesian optimization (BO) is a popular technique for sample-efficient optimization of black-box functions. In many applications, the parameters being tuned come with a carefully engineered default configuration, and practitioners only want to deviate from this default when necessary. Standard BO, however, does not aim to minimize deviation from the default and, in practice, often pushes weakly relevant parameters to the boundary of the search space. This makes it difficult to distinguish between important and spurious changes and increases the burden of vetting recommendations when the optimization objective omits relevant operational considerations. We introduce BONSAI, a default-aware BO policy that prunes low-impact deviations from a default configuration while explicitly controlling the loss in acquisition value. BONSAI is compatible with a variety of acquisition functions, including expected improvement and upper confidence bound (GP-UCB). We theoretically bound the regret incurred by BONSAI, showing that, under certain conditions, it enjoys the same no-regret property as vanilla GP-UCB. Moreover, assuming known ARD lengthscales—the same assumption underlying GP-UCB regret bounds—BONSAI provably recovers the relevant-coordinate set at zero acquisition cost, yielding a method that matches the GP-UCB regret rate while recovering the minimal- ℓ_0 solution—a guarantee not provided by prior sparse-BO methods. Across many real-world applications, we empirically find that BONSAI substantially reduces the number of non-default parameters in recommended configurations while maintaining competitive optimization performance, with little effect on wall time—averaging only $1.5\times$ the candidate-generation cost of standard BO, compared to $7\text{--}34\times$ on average for prior sparse-BO methods (IR, ER, and SEBO).

1 Introduction

Bayesian optimization (BO) [Garnett, 2023] has become a popular approach for optimizing expensive and noisy black-box functions, with applications ranging from hyperparameter tuning to physical experiment design and system configuration. BO relies on a probabilistic surrogate model of an unknown objective f , which is used in an acquisition function to select informative points to evaluate next.

In many of these applications, there is a distinguished *default* or *status quo* configuration. For instance, production systems often ship with carefully tuned configurations, compiler flags, or model-serving infrastructure. Deviating from such defaults can be costly: changing many parameters at once can introduce unintended behaviors that are not captured in the optimization objective and can increase technical debt [Sculley et al., 2015, Liu et al., 2023].

Practitioners, therefore, frequently ask a question that standard BO does not address directly: “*Given a current default configuration, what is the minimal set of changes I can make to optimize my system?*”

*Corresponding author: sdaulton@meta.com

Unfortunately, conventional BO is indifferent to this preference; it typically adjusts many weakly relevant parameters and often pushes marginal dimensions to the boundary of the search space, even when their effect on the objective is negligible.

We propose BONSAI (Bayesian Optimization with Natural Simplicity and Interpretability) to address this gap. BONSAI is a lightweight post-processing layer that sits on top of any acquisition function. At each BO iteration t , BONSAI: 1) identifies a candidate \mathbf{x}_t^* that maximizes the acquisition function α_t , 2) defines the *acquisition gap* $\Delta_t(\mathbf{x}) = \alpha_t(\mathbf{x}_t^*) - \alpha_t(\mathbf{x})$ of any point \mathbf{x} at round t , 3) greedily resets components of \mathbf{x}_t^* back to their default values as long as the acquisition gap of the pruned candidate remains below a relative threshold, and 4) returns the pruned point $\hat{\mathbf{x}}_t$ when any further one-component reset exceeds the threshold. Because BONSAI directly affects the queried points, it is part of the BO decision policy rather than a purely post-hoc analysis.

Contributions.

1. We formalize the setting of *default-aware* BO, where the goal is not only to optimize a black-box function but also to minimize deviation from a specified default configuration, measured by the number of components that change.
2. We introduce BONSAI, a default-aware BO policy that modifies acquisition-maximizing candidates by reverting low-impact deviations to a user-specified default configuration while enforcing a gap rule on the decrease in acquisition value.
3. In the context of using the Upper Confidence Bound (UCB) acquisition function with a Gaussian Process surrogate, we prove that BONSAI’s regret is bounded by the usual GP-UCB term plus a sum of threshold-dependent penalties, the latter of which is controlled under a particular gap rule leading to sublinear regret.
4. We prove a *sparsity-recovery* guarantee: under the same standard ARD lengthscales assumption used in GP-UCB regret bounds, BONSAI prunes every irrelevant coordinate at *zero acquisition cost*, so its returned configuration is supported only on the truly relevant dimensions. Composed with our regret bound, this means BONSAI matches the standard GP-UCB regret rate *while* provably recovering the minimal- ℓ_0 solution. To our knowledge, this is the first such guarantee for default-aware BO; existing sparse-BO methods (IR, ER, SEBO) provide neither a regret bound nor a sparsity-recovery guarantee.
5. We evaluate Expected Improvement (EI) and UCB variants of BONSAI on synthetic and real-world test problems, demonstrating that BONSAI yields favorable sparsity–performance trade-offs: it substantially reduces the number of non-default parameters in the recommended configurations while maintaining competitive optimization performance and wall time relative to standard BO.

2 Background

We briefly review Bayesian optimization (BO), Gaussian process (GP) surrogates, and the GP-UCB algorithm, focusing on the components used in our analysis. We refer to Appendix A and Srinivas et al. [2010] for full details.

Bayesian optimization and GP surrogates. We consider the problem of maximizing an unknown function $f : \mathbb{X} \rightarrow \mathbb{R}$ over a compact domain $\mathbb{X} \subset \mathbb{R}^d$. At iteration t , the algorithm selects a point $\mathbf{x}_t \in \mathbb{X}$, observes a noisy evaluation $y_t = f(\mathbf{x}_t) + \varepsilon_t$, where the noise $\varepsilon_t \sim \mathcal{N}(0, \sigma^2)$ and σ^2 is the noise variance, and uses the history $\{(\mathbf{x}_s, y_s)\}_{s=1}^t$ to decide where to evaluate next. A common choice of surrogate model is a GP prior over f with a constant mean and covariance function k . Conditioned on the data up to time $t - 1$, the GP posterior has mean $\mu_{t-1} : \mathbb{X} \rightarrow \mathbb{R}$ and standard deviation $\sigma_{t-1} : \mathbb{X} \rightarrow \mathbb{R}_+$.

Acquisition functions. BO algorithms typically select \mathbf{x}_t by maximizing an *acquisition function* $\alpha_t : \mathbb{X} \rightarrow \mathbb{R}$ that quantifies the utility of evaluating f at \mathbf{x} given the current posterior. The acquisition balances *exploration* by preferring points with large posterior uncertainty and *exploitation* by preferring points with a large posterior mean. Popular choices include Expected Improvement (EI, Jones et al., 1998), which measures the expected positive improvement over the best observed value so far; Upper Confidence Bound (UCB, Srinivas et al., 2010), which takes the form $\alpha_t^{\text{UCB}}(\mathbf{x}) =$

$\mu_{t-1}(\mathbf{x}) + \beta_t \sigma_{t-1}(\mathbf{x})$, where $\beta_t > 0$ controls the exploration–exploitation trade-off; and information-based criteria such as entropy search [Hennig and Schuler, 2012]. In this paper, BONSAI itself is agnostic to the choice of acquisition function; it only requires the ability to evaluate $\alpha_t(\mathbf{x})$ at candidate points. For our theoretical analysis, we focus on UCB, while in our experiments we also apply BONSAI to EI, which is often more robust in practice [Jones et al., 1998, Shahriari et al., 2016].

3 Related Work

Other related work. *Conservative/safe BO* [e.g., Kazerouni et al., 2017, Sui et al., 2015] constrains the unknown objective relative to a baseline; BONSAI instead constrains the acquisition function and simplifies recommendations in input space, but the two are complementary. *Prior-based BO* methods such as PiBO [Hvarfner et al., 2022] augment the acquisition function with a user-specified prior often centered at a known-good default, providing a soft probabilistic bias toward the default. In contrast, BONSAI imposes a hard ℓ_0 pruning step with explicit acquisition-gap control: rather than reweighting the acquisition surface, it certifies that any deviation from the default contributes meaningfully to the acquisition value. The two are complementary—a PiBO-style prior could be combined with BONSAI pruning. *Variable selection and shrinkage* methods (SAASBO [Eriksson and Jankowiak, 2021], VSBO [Shen and Kingsford, 2023], dimensionality-scaled priors [Hvarfner et al., 2024]) target the surrogate’s structure to improve sample efficiency, but their recommendations can still differ from the default in many components. *Explainable BO* [Chakraborty et al., 2025, Adachi et al., 2024] explains an existing recommendation; BONSAI instead simplifies the recommendation directly. See Appendix F for further discussion.

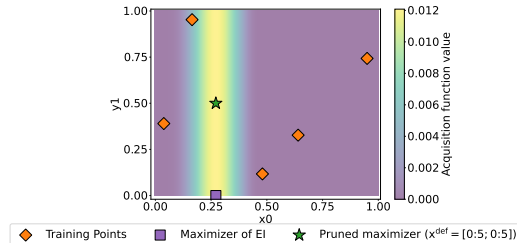


Figure 1: Example where a parameter with no effect (x_1) is sent to the boundary by BO. Even though the effect of x_1 is close to zero, EI is maximized with x_1 on the boundary (purple square). BONSAI mitigates this by moving x_1 back to its default (green star).

METHOD	SINGLE-OBJ.	MULTI-OBJ.
IR- L_0	7.3x ($\pm 8.7x$)	N/A
ER- L_0	8.7x ($\pm 9.2x$)	10.8x ($\pm 14.4x$)
SEBO	13.9x ($\pm 19.1x$)	33.9x ($\pm 61.4x$)
BONSAI EI	1.6x ($\pm 0.8x$)	1.5x ($\pm 0.6x$)

Table 1: Average generation time relative to Vanilla BO across the problems in Sec. 7 (± 2 standard errors over problems), split by single-objective and multi-objective. IR is not applicable to multi-objective settings. Fastest method per column in bold.

Sparse BO. SEBO [Liu et al., 2023] poses sparse BO as learning a sparsity–objective trade-off; we instead optimize the objective and remove low-impact changes from the default. The internal and external regularization (IR/ER) methods of Liu et al. [2023] are most related: IR penalizes the objective by $\|\mathbf{x} - \mathbf{x}^{\text{def}}\|_0$ (requiring acquisition-specific modifications) and ER penalizes the acquisition. Both rely on a hard-to-tune regularization parameter, are non-differentiable due to the ℓ_0 term, and lack theoretical guarantees. They also rely on homotopy continuation, making them substantially more expensive than standard BO: across the benchmarks in Sec. 7, IR/ER/SEBO incur average slowdowns of roughly $7 \times / 9 \times / 14 \times$ over Vanilla BO on single-objective problems (and ER/SEBO incur $11 \times / 34 \times$ on multi-objective; IR is not applicable to multi-objective), with per-problem slowdowns exceeding $25 \times$ (Table 1); BONSAI averages only $1.5 \times - 1.6 \times$ while remaining universally applicable and provably bounding the loss in acquisition value.

Kim et al. [2025] analyze regret under inexact acquisition maximization (a useful tool for our analysis) but do not consider it as a mechanism for simplifying recommendations.

See Appendix F for additional related work.

4 Problem Setting

We now formalize the default-aware BO setting. For clarity, we first consider a single BO iteration and suppress the time index on the acquisition function, writing $\alpha(\cdot)$ to denote the acquisition function in the current iteration. Each configuration $\mathbf{x} \in \mathbb{X} \subset \mathbb{R}^d$ represents a setting of d controllable input parameters, and we refer to x_j as the j -th component of the configuration.

We assume the standard BO setting from Section 2. In addition we are given a fixed *default configuration* $\mathbf{x}^{\text{def}} \in \mathbb{X}$. Intuitively, \mathbf{x}^{def} represents the status quo: a configuration that has been vetted or previously deployed. Deviating from this default can introduce unintended system behaviors or technical debt that is not captured by the primary objective f , and hence, we prefer to deviate from \mathbf{x}^{def} as little as possible.

For any candidate $\mathbf{x} \in \mathbb{X}$, we define its active set $A(\mathbf{x}) := \{j \in \{1, \dots, d\} : x_j \neq \mathbf{x}_j^{\text{def}}\}$, which represents the components in which \mathbf{x} differs from the default. The complexity or deviation of a configuration can thus be measured by its ℓ_0 distance to the default, $\|\mathbf{x} - \mathbf{x}^{\text{def}}\|_0 = |A(\mathbf{x})|$. Our goal is to find a configuration that is both high-performing and sparse relative to the default. This quantity ignores the *magnitude* of the changes and only counts how many coordinates differ from the default, matching our goal of highlighting which parameters need to be touched at all. Formally, we pose this as a relative ϵ -constrained minimal-intervention problem. For a user-specified relative tolerance $\epsilon \in [0, 1)$ on the achievable improvement over the default, the global objective is $\min_{\mathbf{x} \in \mathbb{X}} \|\mathbf{x} - \mathbf{x}^{\text{def}}\|_0$ s.t. $f(\mathbf{x}) \geq f^* - \epsilon(f^* - f(\mathbf{x}^{\text{def}}))$, where $f^* := \max_{\mathbf{x}' \in \mathbb{X}} f(\mathbf{x}')$. Equivalently, ϵ is the fraction of the default-to-optimum improvement we are willing to forgo for sparsity. This defines the ideal target: the configuration with the fewest changed parameters that still achieves near-optimal performance.²

5 Methodology

5.1 Acquisition Gaps and Thresholded Pruning

Solving the global ϵ -objective directly is intractable because f is unknown. BO instead acts on an acquisition function α_t at each iteration t ; without loss of generality we assume α_t is non-negative (any acquisition can be shifted by a constant without changing its maximizer; see Lemma A.1 in Appendix A.1). Let $\mathbf{x}_t^* \in \arg \max_{\mathbf{x} \in \mathbb{X}} \alpha_t(\mathbf{x})$ be its (approximate) maximizer and define the *acquisition gap* of any candidate \mathbf{x} as $\Delta_t(\mathbf{x}) := \alpha_t(\mathbf{x}_t^*) - \alpha_t(\mathbf{x})$. We proxy the global tolerance with a per-iteration relative threshold $\rho_t \in [0, 1)$ on Δ_t . Applying the relative threshold to raw α_t values is not well-posed when the acquisition baseline is arbitrary (e.g., EI vanishes far from data, qLogNEI lives on a log scale), so we instead apply it to a baseline-shifted incremental acquisition $\tilde{\alpha}_t(\mathbf{x}) := \alpha_t(\mathbf{x}) - b_t$, where $b_t := \max_{s < t} \alpha_t(\mathbf{x}_s)$ is the maximum *current-round* acquisition value evaluated across previously queried designs (not the historical acquisition values recorded at query time). This makes ρ_t a fraction of the *improvement over the current best* and renders it comparable across acquisition functions (for log-acquisitions [Ament et al., 2023] we exponentiate before forming b_t ; see Appendix B). Our local per-iteration objective is $\min_{\mathbf{x} \in \mathbb{X}} \|\mathbf{x} - \mathbf{x}^{\text{def}}\|_0$ s.t. $\Delta_t(\mathbf{x}) \leq \rho_t \tilde{\alpha}_t(\mathbf{x}_t^*)$, and Section 6 shows that controlling ρ_t bounds cumulative regret, providing a principled proxy for the global ϵ -objective.

Given $S \subseteq \{1, \dots, d\}$, let $P_S(\mathbf{x})$ be the configuration that keeps components in S as in \mathbf{x} and resets the rest to their defaults. BONSAI restricts to the family of pruned candidates $\mathcal{X}^{\text{prune}} := \{P_S(\mathbf{x}_t^*) : S \subseteq A(\mathbf{x}_t^*)\}$ and selects, within those satisfying the relative gap rule, the one with the smallest active set. Enumerating all $2^{|A(\mathbf{x}_t^*)|}$ subsets is infeasible in high dimensions, so BONSAI uses a greedy algorithm that resets components one at a time. Restricting to single-coordinate resets means BONSAI can miss configurations only reachable by joint resets, but on the low-dimensional problems that we test where enumeration is feasible, this has negligible effect on performance (Section 7).

²Our theory assumes $\mathbb{X} \subset \mathbb{R}^d$ is a compact hyper-rectangle; experiments also use mixed continuous–discrete spaces, where $\|\mathbf{x} - \mathbf{x}^{\text{def}}\|_0$ counts coordinates of any type that differ from the default.

5.2 Sequential Greedy Pruning

Our practical sequential greedy variant (pseudocode in Algorithm 1, Appendix B) initializes $\tilde{\mathbf{x}}_t = \mathbf{x}_t^*$ and repeatedly resets the differing component j whose pruned candidate has the smallest acquisition gap and still satisfies the relative threshold; it stops when no further reset is feasible. The result satisfies the relative-gap condition by construction and matches the exact combinatorial optimum on most low-dimensional problems we test (Section 7). In the worst case, BONSAI performs $O(d^2)$ acquisition evaluations per BO step (at most d outer iterations, each over $|\mathcal{D}| \leq d$ components), which is typically modest relative to α_t -optimization or evaluating f .

6 Theoretical Analysis

We analyze BONSAI in the sequential setting with GP-UCB; complete proofs are in Appendix A.1. Cumulative regret is $R_T = \sum_{t=1}^T [f(\mathbf{x}^*) - f(\mathbf{x}_t)]$ and simple regret $r_T = f(\mathbf{x}^*) - \max_{t \leq T} f(\mathbf{x}_t) \leq R_T/T$, with $\mathbf{x}^* \in \arg \max_{\mathbf{x} \in \mathbb{X}} f(\mathbf{x})$. Under standard kernel regularity [Srinivas et al., 2010], GP-UCB achieves sublinear cumulative regret at the rate $R_T/T = \tilde{O}(\gamma_T/\sqrt{T})$, where γ_T is the maximum information gain. Section 6.1 gives the formal setup, and Section 6.2 expresses our bounds as this GP-UCB term plus an explicit, gap-dependent penalty.

Our bounds depend only on the *acquisition gaps* between queried points and the ideal UCB maximizers, not on how query points are constructed; BONSAI is one such construction that bounds these gaps while minimizing deviations from the default.

6.1 Preliminaries

We work in the standard GP-UCB setting of Srinivas et al. [2010] and adopt the standard GP-UCB assumptions: f lies in the reproducing kernel Hilbert space (RKHS) \mathcal{H}_k associated with a positive definite kernel k , with bounded norm $\|f\|_{\mathcal{H}_k} \leq B$, and the kernel variance is uniformly bounded so that $|f(\mathbf{x})| \leq \kappa B$ for all $\mathbf{x} \in \mathbb{X}$. We place a zero-mean GP prior with covariance k . Under these conditions, the GP posterior after $t-1$ observations has mean μ_{t-1} and standard deviation σ_{t-1} , and GP-UCB uses the acquisition function α_t^{UCB} defined in Section 2. As in the original GP-UCB analysis, we treat the kernel and noise hyperparameters as fixed and known when stating the guarantees; in practice they are typically learned from data.

We write $\mathbf{x}_t^* \in \arg \max_{\mathbf{x} \in \mathbb{X}} \alpha_t(\mathbf{x})$ and denote the maximum acquisition value by $\alpha_t^* := \alpha_t(\mathbf{x}_t^*)$. Following Kim et al. [2025], we define the (multiplicative) *acquisition accuracy* at round t as $\eta_t := \alpha_t(\tilde{\mathbf{x}}_t)/\alpha_t^* \in [0, 1]$, and the *worst-case accumulated inaccuracy* $M_T := \sum_{t=1}^T (1 - \tilde{\eta}_t) \in [0, T]$, where $\tilde{\eta}_t \leq \eta_t$ is any deterministic lower bound on the overall acquisition accuracy at round t (capturing both inner acquisition optimization and BONSAI’s pruning). Intuitively, $1 - \eta_t$ measures the (relative) loss in acquisition value at round t , and M_T aggregates these losses across time. To make BONSAI’s relative rule well-posed, we use the incremental acquisition $\tilde{\alpha}_t(\mathbf{x}) := \alpha_t(\mathbf{x}) - b_t$ with $b_t := \max_{s < t} \alpha_t(\mathbf{x}_s) \geq 0$, and apply thresholds using $\tilde{\alpha}_t(\mathbf{x}_t^*) = \alpha_t^* - b_t$.

Our goal is to characterize how the (possibly zero) acquisition gap incurred by simplifying $\tilde{\mathbf{x}}_t$ relative to the default affects cumulative regret.

6.2 Regret Bounds for BONSAI with GP-UCB

We assume that at each round t the point $\tilde{\mathbf{x}}_t$ selected by the BO policy satisfies a gap rule relative to \mathbf{x}_t^* : $\Delta_t(\tilde{\mathbf{x}}_t) \leq \rho_t \tilde{\alpha}_t(\mathbf{x}_t^*)$ for some user-specified sequence $(\rho_t)_{t \geq 1}$, where $\rho_t \in [0, 1]$. Intuitively, ρ_t is the fraction of acquisition value we are willing to sacrifice at time t in order to simplify the configuration. We begin by bounding the accumulated acquisition inaccuracies in terms of ρ_t (Lemma A.1 in Appendix A.1). Leveraging this lower bound, we obtain the following regret bound for BONSAI with GP-UCB.

Theorem 6.1 (Regret bound via accumulated inaccuracy). *Assume the GP-UCB setting and kernel regularity conditions of Srinivas et al. [2010] and Kim et al. [2025]: in particular, $f \in \mathcal{H}_k$ with $\|f\|_{\mathcal{H}_k} \leq B$, $k(x, x) \leq 1$, and the noise is conditionally R -sub-Gaussian. Let $\alpha_t(\mathbf{x}) = \mu_{t-1}(\mathbf{x}) + \beta_t \sigma_{t-1}(\mathbf{x})$ be the GP-UCB acquisition with $\beta_t = B + R\sqrt{2(\gamma_{t-1} + 1 + \log(1/\delta))}$, where $\delta \in (0, 1]$.*

Suppose that at round t BONSAI returns $\tilde{\mathbf{x}}_t$ satisfying the relative rule $\Delta_t(\tilde{\mathbf{x}}_t) \leq \rho_t \tilde{\alpha}_t(\mathbf{x}_t^*)$, where $\rho_t \in [0, 1)$. Let γ_T denote the maximum information gain after T evaluations. Then, with probability at least $1 - \delta$,

$$R_T = O\left(\gamma_T \sqrt{T} + \sqrt{\gamma_T} \sum_{t=1}^T \rho_t\right). \quad (1)$$

The bound is the standard GP-UCB rate plus an additive penalty proportional to $\sum_t \rho_t$: each round we sacrifice up to a fraction ρ_t of acquisition value for sparsity, and pay a corresponding regret penalty. Under appropriate conditions on $(\rho_t)_{t \geq 1}$, BONSAI remains asymptotically no-regret.

Corollary 6.2 (Asymptotic No-Regret). *If the relative thresholds satisfy $\sum_{t=1}^{\infty} \rho_t < \infty$ or more generally $\sum_{t=1}^T \rho_t = O(\sqrt{T})$, then BONSAI remains asymptotically no-regret and preserves the standard GP-UCB rate up to lower-order terms.*

For example, using $\rho_t = \frac{c}{t}$, where $c > 0$ satisfies Corollary 6.2 when used with squared exponential or Matérn kernels (see Corollary A.2 in Appendix A for formal examples and bounds).

Sparsity recovery guarantees. Under exact ARD lengthscale estimation—the same assumption underlying GP-UCB regret bounds [Srinivas et al., 2010, Kim et al., 2025]—BONSAI prunes every irrelevant coordinate at *zero acquisition cost* (Theorem A.9 in Appendix A.3; we additionally prove recovery under additive acquisitions, Theorem A.12). The result below uses two assumptions (full statements in Appendix A.3):

- **(Perfect ARD lengthscales, A.A.7).** $\ell_j = \infty$ for every irrelevant coordinate $j \notin A^*$, and $\ell_j < \infty$ for $j \in A^*$.
- **(Relevant-dimension gap, A.A.8).** At each round t , $\tau_t := \rho_t \tilde{\alpha}_t(\mathbf{x}_t^*) < \min_{j \in A^* \cap A(\mathbf{x}_t^*)} \Delta_t(R_{S_{\text{irrel}} \cup \{j\}}(\mathbf{x}_t^*))$, where $S_{\text{irrel}} := A(\mathbf{x}_t^*) \setminus A^*$ — i.e., resetting any one relevant coordinate alongside the irrelevant ones costs more than τ_t .

Composing the recovery guarantee with Theorem 6.1 yields:

Proposition 6.3 (BONSAI matches GP-UCB regret while solving the global ϵ -objective). *Suppose the GP-UCB regret assumptions of Srinivas et al. [2010] and Assumption A.7 hold. Let $\{\rho_t\}_{t \geq 1}$ be any threshold schedule with $\rho_t \geq 0$ such that, at every round t , either (a) $\rho_t = 0$, or (b) Assumption A.8 holds. Then:*

1. (Sparsity recovery) *For every round t , $A(\tilde{\mathbf{x}}_t) \subseteq A^* := \{j : \ell_j < \infty\}$; in particular $\|\tilde{\mathbf{x}}_t - \mathbf{x}^{\text{def}}\|_0 \leq |A^*|$.*
2. (No-cost pruning) *Pruning every irrelevant coordinate incurs zero acquisition gap, so $\Delta_t(\tilde{\mathbf{x}}_t) = 0$ at every round and BONSAI's cumulative regret satisfies the standard GP-UCB rate $\tilde{O}(\sqrt{T\gamma_T})$ without the additive $\mathcal{O}(\sqrt{\gamma_T} \sum_t \rho_t)$ penalty in Theorem 6.1.*
3. (Global ϵ -objective) *Standard GP-UCB regret bounds imply $f^* - f(\hat{\mathbf{x}}_T) \leq \tilde{O}(\sqrt{\gamma_T/T})$ for the best historical point $\hat{\mathbf{x}}_T \in \arg \max_{t \leq T} f(\tilde{\mathbf{x}}_t)$. Combined with sparsity recovery (Claim 1), $\hat{\mathbf{x}}_T$ is feasible for the global relative ϵ_T -constrained minimal-intervention problem of Section 5 with $\epsilon_T = \tilde{O}(\sqrt{\gamma_T/T}) / (f^* - f(\mathbf{x}^{\text{def}})) \rightarrow 0$, and $\|\hat{\mathbf{x}}_T - \mathbf{x}^{\text{def}}\|_0 \leq |A^*|$ matches the ideal minimal- ℓ_0 solution restricted to A^* .*

In practice, lengthscales are finite but large enough for BONSAI to recover sparse structure on real problems (e.g., Optical Design uses $< 50\%$ of its 146 parameters; Appendix C.12).

6.3 Extensions

Batch candidate generation. In settings where multiple points are evaluated in parallel at each BO iteration, one typically maximizes a batch acquisition function $\alpha : \mathbb{X}^q \rightarrow \mathbb{R}$ over tuples $X = (\mathbf{x}_1, \dots, \mathbf{x}_q)$. BONSAI can be extended to this setting by applying the pruning procedure to each point in the batch while conditioning on the previously selected pruned batch entries. In the batch setting, we use the incremental acquisition function described in Section 5.1 when pruning the first point. For pruning subsequent points, we use the incremental improvement over the previously selected and pruned points in the batch.

Acquisition functions. Our theoretical results are specific to the GP-UCB acquisition. BONSAI itself, however, is purely a post-processing step that only requires the ability to evaluate an acquisition function at candidate points. In particular, it can be used with EI and its variants, which we find to be more robust in some of our empirical studies. In those cases, the regret guarantees in Section 6 should be viewed as a guide rather than a formal guarantee: they capture what happens if one could construct an acquisition function with analogous confidence properties and bounded gaps.

7 Experiments

We evaluate BONSAI on a variety of synthetic and real-world benchmark problems. We compare against the following baselines: quasi-random Sobol sampling, standard BO (EI), and three methods for sparse BO from Liu et al. [2023]: IR, ER, and SEBO. For IR/ER, we use an ℓ_0 penalty coefficient of 0.01, which is reported in SEBO as a strong default choice.³ See Appendix C.11 for a sensitivity analysis of IR and ER. All methods use the same MAP-SAAS GP surrogate: a GP with a Matérn-5/2 kernel with a SAAS prior [Eriksson and Jankowiak, 2021], where the GP hyperparameters are fit with a novel sampling and MAP estimation approach to speed up model fitting (see Appendix D for details).

We initialize each method by evaluating the default point x^{def} and 20 Sobol samples. We leverage qLogNEI and qLogNEHVI [Ament et al., 2023] as the EI-based acquisition functions for all methods for single- and multi-objective problems, respectively. For BONSAI with EI, we use a fixed relative threshold $\rho = 0.2$ —matching the configuration whose sensitivity is analyzed in Appendix C.8—while for BONSAI with UCB we use the theoretical schedule $\rho_t = 1/t$ from Corollary A.2. To apply UCB to multi-objective problems, we use random hypervolume scalarizations [Zhang and Golovin, 2020], which scalarize the multi-objective acquisition into a single-objective UCB at each iteration. Appendix C.7 provides a head-to-head comparison and shows EI and UCB perform comparably on most problems. All methods are implemented using Ax [Olson et al., 2025] with components from BoTorch [Balandat et al., 2020]; BONSAI code is available at <https://ax.dev/>.

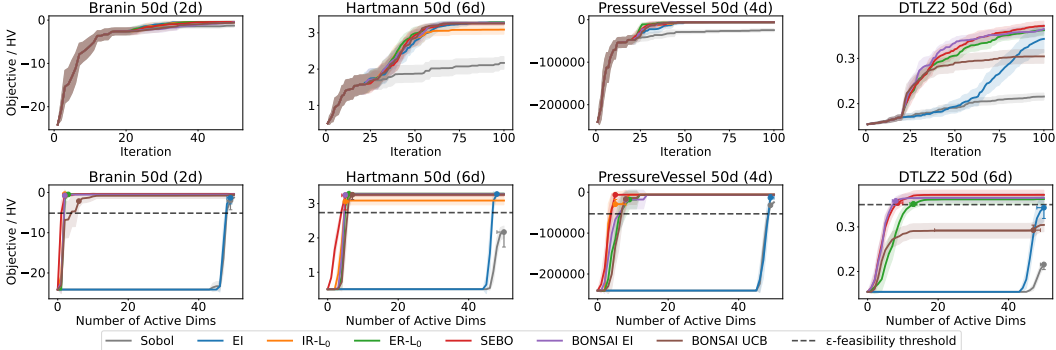


Figure 2: Top row: Objective or HV. Bottom row: Best Objective (or HV) value for each level of active dimensions. For MOO, the HV at sparsity level k is the hypervolume of the feasible Pareto frontier computed over all evaluated points with at most k active dimensions.

7.1 Benchmarks

Our test problems include single-objective, constrained, and multi-objective settings. All problems are maximization problems—we negate the objective for minimization problems. We report optimization performance (best observed feasible objective for constrained problems and hypervolume (HV) for multi-objective problems) and candidate generation time—acquisition optimization and pruning (for BONSAI)—in sequential ($q = 1$) settings. See Appendix C.6 for results in batch ($q = 5$) settings.

In typical default-aware BO applications, the search space is centered around the default (status quo) configuration: practitioners explore perturbations from a known-good configuration. Our

³IR and ER were proposed in Liu et al. [2023] for single-objective optimization, but we extend both to constrained optimization, and we extend ER to multi-objective optimization. See Appendix E for further discussion.

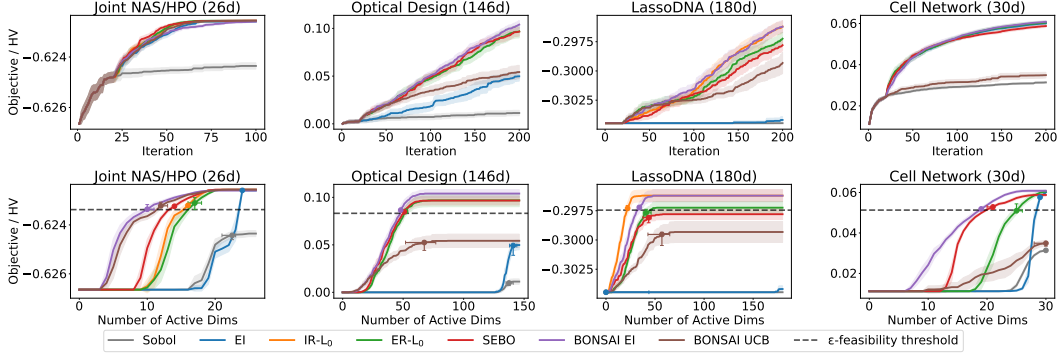


Figure 3: Top row: objective or HV. Bottom row: Best Objective (or HV) value for each level of active dimensions. For MOO, the HV at sparsity level k is the hypervolume of the feasible Pareto frontier computed over all evaluated points with at most k active dimensions.

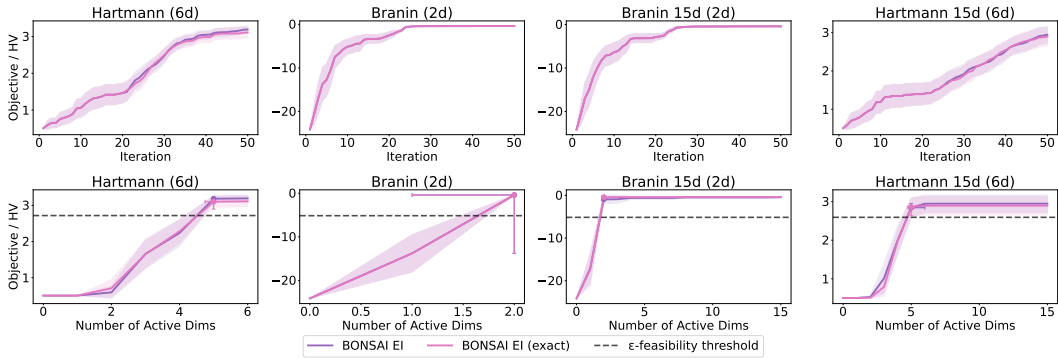


Figure 4: All methods (Sobol, Vanilla BO, IR, ER, SEBO, and BONSAI EI with sequential greedy and exact pruning) on low-dimensional problems where exact pruning is computationally feasible (cost $O(2^{|A(\mathbf{x}_i^*)|})$). BONSAI’s greedy and exact variants yield comparable optimization performance, and BONSAI is competitive with the default-aware baselines. On Branin (2d), the BONSAI greedy and exact traces overlap exactly (both pruning strategies coincide at $d = 2$). Top row: Objective. Bottom row: Best Objective value for each level of active dimensions.

ranking system benchmarks (Appendix C.5.1) exemplify this directly—the defaults correspond to the control configuration in surrogates of real-world A/B tests, which is the production system status quo. LassoDNA also has a meaningful default (zero penalty). For synthetic benchmarks (e.g., Hartmann embedded in 50 dimensions), we set \mathbf{x}^{def} to be the center of the search space, reflecting the common practical scenario where search bounds are defined symmetrically around the current operating point.

Synthetic. Branin (2d), Hartmann (6d), PressureVessel (4d, 4 constraints) [Coello Coello and Mezura Montes, 2002], and DTLZ2 (6d, 2-objective) [Deb et al., 2002], each embedded in a 50d search space by adding irrelevant parameters.

Real-world. (i) *Joint NAS/HPO* (26d, mixed integer/continuous): a GP surrogate of a multi-task, multi-label neural network architecture/HPO problem at a large web service. (ii) *Optical Design* (146d, 2-objective) [Daulton et al., 2022]: surface morphology and geometry of an AR see-through display, evaluated via a neural network surrogate of physical simulations. (iii) *LassoDNA* (180d) [Šehić et al., 2022]: per-feature weighted-Lasso penalties on the DNA dataset [Chang and Lin, 2011]. (iv) *Cell Network* (30d, mixed, 2-objective) [Dreifuerst et al., 2021]: per-antenna transmission power and downtilt, minimizing under- and over-coverage. See Appendix C for full descriptions and additional benchmarks (including noisy real-world ranking problems).

7.2 Results

We report optimization performance over the number of evaluations, the best objective found for a given number of active dimensions, and candidate generation time. For multi-objective problems, we report, for each sparsity level $k = 0, \dots, D$, the hypervolume of the feasible Pareto frontier formed by all evaluated points with at most k active dimensions (i.e., $\|\mathbf{x} - \mathbf{x}^{\text{def}}\|_0 \leq k$). We report the mean and ± 2 standard errors across 20 replications. In the bottom row of Figures 2 and 3, we overlay a marker per method summarizing each replication’s *minimal-intervention solution*: the sparsest explored configuration satisfying the relative ϵ -constraint of Section 4 at $\epsilon = 0.2$ (i.e., within 20% of the default-to-optimum improvement); for multi-objective problems, an analogous hypervolume-based criterion is used (defined in Appendix C). Since these per-replication points are bounded and skewed, each is first snapped to the closest point on the method’s mean PF, and we plot the median across replications with 25th–75th percentile error bars in both sparsity and objective. These markers operationalize the global ϵ -constrained objective from Section 5 for a concrete choice of ϵ .

Across all benchmarks, we find that BONSAI yields consistently favorable sparsity–performance trade-offs: it produces substantially simpler recommendations while maintaining competitive performance with respect to the objective (or hypervolume), and it is typically the fastest default-aware method with respect to generation time. The minimal-intervention markers make this concrete: BONSAI’s median solution sits consistently to the lower-left of the alternatives (fewer active dimensions while still ϵ -feasible), with IQR bars confirming the gap is robust across replications. SEBO produces sparse solutions but at significantly higher wall-time cost than BONSAI, with no consistent advantage in sparsity–quality trade-off and substantially worse performance on mixed-discrete problems. On synthetic benchmarks in Figure 2, BONSAI recovers near-optimal solutions at or close to the true number of relevant parameters; standard BO achieves strong objective values via dense changes, while BONSAI yields better objective/HV at comparable sparsity. IR and ER also find near-optimal sparse solutions, but IR fails on Hartmann 50d, and BONSAI outperforms ER on DTLZ2 50d.

On the real problems in Figure 3, results are similar. The real problems have significant numbers of irrelevant parameters: e.g., on Optical Design, BONSAI finds excellent Pareto frontiers using an average of fewer than 60 active dimensions ($< 50\%$ of the parameters). On DTLZ2, Optical Design, and LassoDNA, BONSAI outperforms standard BO, which we attribute to its sparser candidates improving lengthscale estimation (Figure 18 in Appendix C.12). BONSAI’s candidate generation time is on-par with standard BO, while IR/ER/SEBO are substantially slower (Table 2; see Appendix C for additional notes on per-problem wall-time anomalies, omitted batch runs, and the active-dimension tolerance used for continuous-relaxation baselines). On lower-dimensional benchmarks where exact pruning is feasible, all methods are evaluated and BONSAI’s optimization performance is comparable to Vanilla BO with EI and to the default-aware baselines (Figure 4; full results in Appendix C.9).

Greedy versus exact pruning. Greedy may in principle miss joint-reset configurations, but this is mitigated both theoretically (Proposition 6.3) and empirically: on every low-dimensional problem where exact $O(2^{|\mathcal{A}(\mathbf{x}^*)|})$ enumeration is feasible, greedy and exact pruning yield comparable performance and return the same first candidate 85.7% of the time (Appendix C.9). Exact pruning is infeasible at the scales of our main experiments.

8 Discussion

BONSAI is a lightweight, default-aware BO policy that simplifies recommendations by minimizing deviations from a default subject to an acquisition-gap constraint, yielding solutions that are easier to inspect, test, and deploy than unconstrained BO candidates. For GP-UCB it can be viewed as inexact acquisition maximization [Kim et al., 2025], with cumulative regret matching standard GP-UCB up to an additive penalty whenever accumulated inaccuracy grows sublinearly. BONSAI measures simplicity via coordinate-wise ℓ_0 distance, natural for independently actionable knobs; structured or grouped sparsity is a promising extension. Other directions include finite-sample sparsity recovery under imperfect lengthscale estimation, extending the regret analysis to EI, and combining BONSAI with post-hoc explanation methods (Appendix G).

Impact Statement

This work aims to improve the usability and interpretability of Bayesian optimization in applications where there is a meaningful default configuration and where changing many parameters at once can be risky or costly from an operational perspective. By encouraging recommendations that change as few input parameters as possible relative to the default, BONSAI may help practitioners deploy BO in operationally constrained settings, such as large-scale systems configuration or model serving infrastructure.

At the same time, BONSAI is not a substitute for careful specification of objectives and constraints: if important aspects of system behavior are omitted from the optimization objective, BO—with or without BONSAI—may still propose configurations that are undesirable in practice. We therefore view BONSAI as a complementary tool that can make it easier for practitioners to inspect and reason about BO suggestions, but it should be used in conjunction with domain expertise, monitoring, and appropriate validation checks.

References

- Masaki Adachi, Brady Planden, David Howey, Michael A. Osborne, Sebastian Orbell, Natalia Ares, Krikamol Muandet, and Siu Lun Chau. Looping in the human: Collaborative and explainable Bayesian optimization. In Sanjoy Dasgupta, Stephan Mandt, and Yingzhen Li, editors, *Proceedings of The 27th International Conference on Artificial Intelligence and Statistics*, volume 238 of *Proceedings of Machine Learning Research*, pages 505–513. PMLR, 02–04 May 2024. URL <https://proceedings.mlr.press/v238/adachi24a.html>.
- Sebastian Ament, Samuel Daulton, David Eriksson, Maximilian Balandat, and Eytan Bakshy. Unexpected improvements to expected improvement for bayesian optimization. In A. Oh, T. Naumann, A. Globerson, K. Saenko, M. Hardt, and S. Levine, editors, *Advances in Neural Information Processing Systems*, volume 36, pages 20577–20612. Curran Associates, Inc., 2023.
- Maximilian Balandat, Brian Karrer, Daniel R. Jiang, Samuel Daulton, Benjamin Letham, Andrew Gordon Wilson, and Eytan Bakshy. BoTorch: A Framework for Efficient Monte-Carlo Bayesian Optimization. In *Advances in Neural Information Processing Systems 33*, 2020.
- Tanmay Chakraborty, Christian Wirth, and Christin Seifert. Explainable bayesian optimization, 2025. URL <https://arxiv.org/abs/2401.13334>.
- Chih-Chung Chang and Chih-Jen Lin. Libsvm: A library for support vector machines. *ACM Trans. Intell. Syst. Technol.*, 2(3), May 2011. ISSN 2157-6904. doi: 10.1145/1961189.1961199. URL <https://doi.org/10.1145/1961189.1961199>.
- Carlos A. Coello Coello and Efrén Mezura Montes. Constraint-handling in genetic algorithms through the use of dominance-based tournament selection. *Advanced Engineering Informatics*, 16(3):193–203, 2002. ISSN 1474-0346. doi: [https://doi.org/10.1016/S1474-0346\(02\)00011-3](https://doi.org/10.1016/S1474-0346(02)00011-3). URL <https://www.sciencedirect.com/science/article/pii/S1474034602000113>.
- Sam Daulton, Maximilian Balandat, and Eytan Bakshy. Hypervolume knowledge gradient: A lookahead approach for multi-objective Bayesian optimization with partial information. In Andreas Krause, Emma Brunskill, Kyunghyun Cho, Barbara Engelhardt, Sivan Sabato, and Jonathan Scarlett, editors, *Proceedings of the 40th International Conference on Machine Learning*, volume 202 of *Proceedings of Machine Learning Research*, pages 7167–7204. PMLR, 23–29 Jul 2023. URL <https://proceedings.mlr.press/v202/daulton23a.html>.
- Samuel Daulton, Maximilian Balandat, and Eytan Bakshy. Differentiable expected hypervolume improvement for parallel multi-objective bayesian optimization. In *Proceedings of the 34th International Conference on Neural Information Processing Systems*, NIPS ’20, Red Hook, NY, USA, 2020. Curran Associates Inc. ISBN 9781713829546.
- Samuel Daulton, Maximilian Balandat, and Eytan Bakshy. Parallel bayesian optimization of multiple noisy objectives with expected hypervolume improvement. In *Proceedings of the 35th International Conference on Neural Information Processing Systems*, NIPS ’21, Red Hook, NY, USA, 2021. Curran Associates Inc. ISBN 9781713845393.

- Samuel Daulton, David Eriksson, Maximilian Balandat, and Eytan Bakshy. Multi-objective bayesian optimization over high-dimensional search spaces. In James Cussens and Kun Zhang, editors, *Proceedings of the Thirty-Eighth Conference on Uncertainty in Artificial Intelligence*, volume 180 of *Proceedings of Machine Learning Research*, pages 507–517. PMLR, 01–05 Aug 2022. URL <https://proceedings.mlr.press/v180/daulton22a.html>.
- Kalyan Deb, L. Thiele, Marco Laumanns, and Eckart Zitzler. Scalable multi-objective optimization test problems. volume 1, pages 825–830, 06 2002. ISBN 0-7803-7282-4. doi: 10.1109/CEC.2002.1007032.
- Ryan M Dreifuerst, Samuel Daulton, Yuchen Qian, Paul Varkey, Maximilian Balandat, Sanjay Kasturia, Anoop Tomar, Ali Yazdan, Vish Ponnampalam, and Robert W Heath. Optimizing coverage and capacity in cellular networks using machine learning. In *ICASSP 2021-2021 IEEE International Conference on Acoustics, Speech and Signal Processing (ICASSP)*, pages 8138–8142. IEEE, 2021.
- David Eriksson and Martin Jankowiak. High-dimensional Bayesian optimization with sparse axis-aligned subspaces. In Cassio de Campos and Marloes H. Maathuis, editors, *Proceedings of the Thirty-Seventh Conference on Uncertainty in Artificial Intelligence*, volume 161 of *Proceedings of Machine Learning Research*, pages 493–503. PMLR, 27–30 Jul 2021. URL <https://proceedings.mlr.press/v161/eriksson21a.html>.
- Qing Feng, Samuel Daulton, Benjamin Letham, Maximilian Balandat, and Eytan Bakshy. Experimenting, fast and slow: Bayesian optimization of long-term outcomes with online experiments. In *Proceedings of the 31st ACM SIGKDD Conference on Knowledge Discovery and Data Mining V.1*, KDD '25, page 2235–2246, New York, NY, USA, 2025. Association for Computing Machinery. ISBN 9798400712456. doi: 10.1145/3690624.3709419. URL <https://doi.org/10.1145/3690624.3709419>.
- Roman Garnett. *Bayesian Optimization*. Cambridge University Press, 2023.
- Philipp Hennig and Christian J. Schuler. Entropy search for information-efficient global optimization. *J. Mach. Learn. Res.*, 13(null):1809–1837, June 2012. ISSN 1532-4435.
- Carl Hvarfner, Danny Stoll, Artur Souza, Luigi Nardi, Marius Lindauer, and Frank Hutter. Augmenting acquisition functions with user beliefs for bayesian optimization. In *International Conference on Learning Representations*, 2022. URL <https://openreview.net/forum?id=MMAeCXIa89>.
- Carl Hvarfner, Erik Orm Hellsten, and Luigi Nardi. Vanilla Bayesian optimization performs great in high dimensions. In Ruslan Salakhutdinov, Zico Kolter, Katherine Heller, Adrian Weller, Nuria Oliver, Jonathan Scarlett, and Felix Berkenkamp, editors, *Proceedings of the 41st International Conference on Machine Learning*, volume 235 of *Proceedings of Machine Learning Research*, pages 20793–20817. PMLR, 21–27 Jul 2024.
- Carl Hvarfner, David Eriksson, Eytan Bakshy, and Max Balandat. Informed initialization for bayesian optimization and active learning. *arXiv preprint arXiv:2510.23681*, 2025.
- Donald R. Jones, Matthias Schonlau, and William J. Welch. Efficient global optimization of expensive black-box functions. *Journal of Global Optimization*, 13:455–492, 1998.
- Kirthevasan Kandasamy, Jeff Schneider, and Barnabas Poczos. High dimensional bayesian optimization and bandits via additive models. In *Proceedings of the 32nd International Conference on Machine Learning*, volume 37 of *Proceedings of Machine Learning Research*, pages 295–304. PMLR, 2015.
- Abbas Kazerouni, Mohammad Ghavamzadeh, Yasin Abbasi-Yadkori, and Benjamin Van Roy. Conservative contextual linear bandits. In *Proceedings of the 31st International Conference on Neural Information Processing Systems, NIPS'17*, page 3913–3922, Red Hook, NY, USA, 2017. Curran Associates Inc. ISBN 9781510860964.

- Hwanwoo Kim, Chong Liu, and Yuxin Chen. Bayesian optimization with inexact acquisition: Is random grid search sufficient? In Silvia Chiappa and Sara Magliacane, editors, *Proceedings of the Forty-first Conference on Uncertainty in Artificial Intelligence*, volume 286 of *Proceedings of Machine Learning Research*, pages 2202–2222. PMLR, 21–25 Jul 2025. URL <https://proceedings.mlr.press/v286/kim25b.html>.
- Chi-Heng Lin, Joseph D. Miano, and Eva L. Dyer. Bayesian optimization for modular black-box systems with switching costs. In Cassio de Campos and Marloes H. Maathuis, editors, *Proceedings of the Thirty-Seventh Conference on Uncertainty in Artificial Intelligence*, volume 161 of *Proceedings of Machine Learning Research*, pages 1024–1034. PMLR, 27–30 Jul 2021. URL <https://proceedings.mlr.press/v161/lin21c.html>.
- Sulin Liu, Qing Feng, David Eriksson, Benjamin Letham, and Eytan Bakshy. Sparse bayesian optimization. In Francisco Ruiz, Jennifer Dy, and Jan-Willem van de Meent, editors, *Proceedings of The 26th International Conference on Artificial Intelligence and Statistics*, volume 206 of *Proceedings of Machine Learning Research*, pages 3754–3774. PMLR, 25–27 Apr 2023. URL <https://proceedings.mlr.press/v206/liu23b.html>.
- Miles Olson, Elizabeth Santorella, Louis C. Tiao, Sait Cakmak, David Eriksson, Mia Garrard, Sam Daulton, Maximilian Balandat, Eytan Bakshy, Elena Kashtelyan, Zhiyuan Jerry Lin, Sebastian Ament, Bernard Beckerman, Eric Onofrey, Paschal Igusti, Cristian Lara, Benjamin Letham, Cesar Cardoso, Shiyun Sunny Shen, Andy Chenyuan Lin, and Matthew Grange. Ax: A platform for adaptive experimentation. In *AutoML 2025 ABCD Track*, 2025. URL <https://openreview.net/forum?id=U1f6wHtG1g>.
- D. Sculley, Gary Holt, Daniel Golovin, Eugene Davydov, Todd Phillips, Dietmar Ebner, Vinay Chaudhary, Michael Young, Jean-Francois Crespo, and Dan Dennison. Hidden technical debt in machine learning systems. In *Proceedings of the 29th International Conference on Neural Information Processing Systems - Volume 2, NIPS’15*, page 2503–2511, Cambridge, MA, USA, 2015. MIT Press.
- Kenan Šehić, Alexandre Gramfort, Joseph Salmon, and Luigi Nardi. Lassobench: A high-dimensional hyperparameter optimization benchmark suite for lasso. In *First Conference on Automated Machine Learning (Main Track)*, 2022. URL <https://openreview.net/forum?id=S41eJbTrLg5>.
- Bobak Shahriari, Kevin Swersky, Ziyu Wang, Ryan P. Adams, and Nando de Freitas. Taking the human out of the loop: A review of bayesian optimization. *Proceedings of the IEEE*, 104(1): 148–175, 2016. doi: 10.1109/JPROC.2015.2494218.
- Yihang Shen and Carl Kingsford. Computationally efficient high-dimensional bayesian optimization via variable selection. In Aleksandra Faust, Roman Garnett, Colin White, Frank Hutter, and Jacob R. Gardner, editors, *Proceedings of the Second International Conference on Automated Machine Learning*, volume 224 of *Proceedings of Machine Learning Research*, pages 15/1–27. PMLR, 12–15 Nov 2023. URL <https://proceedings.mlr.press/v224/shen23a.html>.
- Lei Song, Ke Xue, Xiaobin Huang, and Chao Qian. Monte carlo tree search based variable selection for high dimensional bayesian optimization. In *Proceedings of the 36th International Conference on Neural Information Processing Systems, NIPS ’22*, Red Hook, NY, USA, 2022. Curran Associates Inc. ISBN 9781713871088.
- Niranjan Srinivas, Andreas Krause, Sham Kakade, and Matthias Seeger. Gaussian process optimization in the bandit setting: No regret and experimental design. In *Proceedings of the 27th International Conference on International Conference on Machine Learning, ICML’10*, page 1015–1022, Madison, WI, USA, 2010. Omnipress. ISBN 9781605589077.
- Yanan Sui, Alkis Gotovos, Joel Burdick, and Andreas Krause. Safe exploration for optimization with gaussian processes. In Francis Bach and David Blei, editors, *Proceedings of the 32nd International Conference on Machine Learning*, volume 37 of *Proceedings of Machine Learning Research*, pages 997–1005, Lille, France, 07–09 Jul 2015. PMLR. URL <https://proceedings.mlr.press/v37/sui15.html>.

- Sebastian Tay, Chuan Sheng Foo, Daisuke Urano, Richalynn Leong, and Bryan Kian Hsiang Low. Bayesian optimization with cost-varying variable subsets. In A. Oh, T. Naumann, A. Globerson, K. Saenko, M. Hardt, and S. Levine, editors, *Advances in Neural Information Processing Systems*, volume 36, pages 3008–3031. Curran Associates, Inc., 2023.
- Sattar Vakili, Kia Khezeli, and Victor Picheny. On information gain and regret bounds in gaussian process bandits. In Arindam Banerjee and Kenji Fukumizu, editors, *Proceedings of The 24th International Conference on Artificial Intelligence and Statistics*, volume 130 of *Proceedings of Machine Learning Research*, pages 82–90. PMLR, 13–15 Apr 2021. URL <https://proceedings.mlr.press/v130/vakili21a.html>.
- Richard Zhang and Daniel Golovin. Random hypervolume scalarizations for provable multi-objective black box optimization. In Hal Daumé III and Aarti Singh, editors, *Proceedings of the 37th International Conference on Machine Learning*, volume 119 of *Proceedings of Machine Learning Research*, pages 11096–11105. PMLR, 13–18 Jul 2020. URL <https://proceedings.mlr.press/v119/zhang20i.html>.

A Proofs and Additional Theoretical Results

A.1 Proofs

Lemma A.1 (Relative rule implies accuracy lower bound). *Using BONSAI at round t , the acquisition accuracy satisfies $\eta_t \geq 1 - \rho_t$. Consequently we may take $\tilde{\eta}_t := 1 - \rho_t$ in the definition of M_T (assuming exact inner maximization), and the worst-case accumulated inaccuracy is bounded by $M_T \leq \sum_{t=1}^T \rho_t$.*

Following Kim et al. [2025], we assume non-negative acquisition functions. This is without loss of generality: any acquisition function can be shifted by a constant to be non-negative without changing the maximizer. Under this convention, $b_t = \max_{s < t} \alpha_t(\mathbf{x}_s) \geq 0$ and $\alpha_t^* > 0$.

Proof. By definition,

$$\Delta_t(\tilde{\mathbf{x}}_t) = \alpha_t(\mathbf{x}_t^*) - \alpha_t(\tilde{\mathbf{x}}_t) \leq \rho_t \tilde{\alpha}_t(\mathbf{x}_t^*).$$

Recalling $\tilde{\alpha}_t(\mathbf{x}_t^*) = \alpha_t(\mathbf{x}_t^*) - b_t$ with $b_t := \max_{s < t} \alpha_t(\mathbf{x}_s) \geq 0$, we have

$$\Delta_t(\tilde{\mathbf{x}}_t) = \alpha_t(\mathbf{x}_t^*) - \alpha_t(\tilde{\mathbf{x}}_t) \leq \rho_t \alpha_t(\mathbf{x}_t^*),$$

and rearranging gives

$$\alpha_t(\tilde{\mathbf{x}}_t) \geq (1 - \rho_t) \alpha_t(\mathbf{x}_t^*).$$

Dividing by $\alpha_t(\mathbf{x}_t^*) = \alpha_t^* > 0$ yields $\eta_t \geq 1 - \rho_t$, and thus $1 - \tilde{\eta}_t \leq \rho_t$ when we choose $\tilde{\eta}_t := 1 - \rho_t$. Summing over t proves the result. \square

Inner optimization accuracy. The argument above treats \mathbf{x}_t^* as an exact maximizer of α_t . If instead an inner solver returns $\hat{\mathbf{x}}_t$ with a guarantee $\alpha_t(\hat{\mathbf{x}}_t) \geq \eta_t^{\text{solve}} \alpha_t^*$ for some $\eta_t^{\text{solve}} \in (0, 1]$, and BONSAI is applied so that $\alpha_t(\tilde{\mathbf{x}}_t) \geq (1 - \rho_t) \alpha_t(\hat{\mathbf{x}}_t)$ on the same nonnegative acquisition scale, then the composite selection satisfies $\alpha_t(\tilde{\mathbf{x}}_t)/\alpha_t^* \geq (1 - \rho_t) \eta_t^{\text{solve}}$ and one may take $\tilde{\eta}_t = (1 - \rho_t) \eta_t^{\text{solve}}$ in the definition of M_T .

Theorem 6.1 (Regret bound via accumulated inaccuracy). *Assume the GP-UCB setting and kernel regularity conditions of Srinivas et al. [2010] and Kim et al. [2025]: in particular, $f \in \mathcal{H}_k$ with $\|f\|_{\mathcal{H}_k} \leq B$, $k(x, x) \leq 1$, and the noise is conditionally R-sub-Gaussian. Let $\alpha_t(\mathbf{x}) = \mu_{t-1}(\mathbf{x}) + \beta_t \sigma_{t-1}(\mathbf{x})$ be the GP-UCB acquisition with $\beta_t = B + R\sqrt{2(\gamma_{t-1} + 1 + \log(1/\delta))}$, where $\delta \in (0, 1]$. Suppose that at round t BONSAI returns $\tilde{\mathbf{x}}_t$ satisfying the relative rule $\Delta_t(\tilde{\mathbf{x}}_t) \leq \rho_t \tilde{\alpha}_t(\mathbf{x}_t^*)$, where $\rho_t \in [0, 1)$. Let γ_T denote the maximum information gain after T evaluations. Then, with probability at least $1 - \delta$,*

$$R_T = O\left(\gamma_T \sqrt{T} + \sqrt{\gamma_T} \sum_{t=1}^T \rho_t\right). \quad (1)$$

Proof. This is a direct specialization of Theorem 3 of Kim et al. [2025] with $\rho_t = 1 - \eta_t$. Using the same exploration schedule β_t , yields (1). \square

Corollary 6.2 (Asymptotic No-Regret). *If the relative thresholds satisfy $\sum_{t=1}^{\infty} \rho_t < \infty$ or more generally $\sum_{t=1}^T \rho_t = O(\sqrt{T})$, then BONSAI remains asymptotically no-regret and preserves the standard GP-UCB rate up to lower-order terms.*

Proof. The asymptotic statement follows by comparing $\sum_{t=1}^T \rho_t$ to \sqrt{T} and using the known growth of γ_T for the kernels considered. \square

Corollary A.2 (Example schedules). *Assume $\gamma_T = O(\log^{d+1} T)$ (SE kernel) or $\gamma_T = O(T^{d/(d+2\nu)} \log^{2\nu/(2\nu+d)}(T))$ (Matérn kernel with smoothness $\nu > \frac{1}{2}$), as in Vakili et al. [2021]. Let $\rho_t = \frac{c}{t^{1+c}}$, where $c > 0$ and $\epsilon > 0$. Then $\sum_{t=1}^{\infty} \rho_t < \infty$ and hence $M_T = O(1)$, so $R_T = O(\gamma_T \sqrt{T})$. More generally, if $\rho_t = c/t$ then $\sum_{t=1}^T \rho_t = O(\log T)$ and*

$$R_T = O\left(\gamma_T \sqrt{T} + \sqrt{\gamma_T} \log T\right),$$

which preserves the standard GP-UCB rate up to logarithmic factors. In both cases BONSAI's relative rule is gradually tightened over time (through decreasing ρ_t), which controls the growth of M_T and guarantees asymptotic optimality.

Proof. For $\rho_t = c/t^{1+\epsilon}$ with $\epsilon > 0$, the series $\sum_{t=1}^{\infty} \rho_t$ converges, so $M_T = O(1)$. Plugging into (1) yields

$$R_T = O(\gamma_T \sqrt{T} + \sqrt{\gamma_T}) = O(\gamma_T \sqrt{T}).$$

For $\rho_t = c/t$, we have $\sum_{t=1}^T \rho_t = c(1 + \log T)$, and (1) gives

$$R_T = O(\gamma_T \sqrt{T} + \sqrt{\gamma_T \log T}).$$

The growth of γ_T for SE and Matérn kernels then yields the stated asymptotics. \square

A.2 Thresholds and Acquisition Gaps: A Toy Additive Model

The regret bounds above characterize the optimization cost of allowing acquisition gaps, but they do not by themselves explain how the thresholds influence the *sparsity* of BONSAI's recommendations. We now give a brief, concrete picture of this interaction for a broad class of ARD kernels that includes both SE-ARD and Matérn-ARD (e.g., Matérn-5/2). This subsection helps explain which coordinates BONSAI tends to prune under common ARD kernels.

We assume an ARD kernel of the form

$$k(\mathbf{x}, \mathbf{x}') = \sigma_f^2 \phi(r(\mathbf{x}, \mathbf{x}')), \quad r(\mathbf{x}, \mathbf{x}') = \sqrt{\sum_{j=1}^d \frac{(x_j - x'_j)^2}{\ell_j^2}},$$

where $\ell_j > 0$ are per-component lengthscales and $\phi : [0, \infty) \rightarrow \mathbb{R}$ is a smooth radial profile such that $r \mapsto r \phi'(r)$ is bounded on $[0, \infty)$. This family includes the SE-ARD kernel (with $\phi(r) = \exp(-\frac{1}{2}r^2)$) and common Matérn-ARD kernels such as Matérn-5/2.

Intuitively, large ℓ_j indicate directions along which the surrogate varies slowly, so we expect changes along those components to have a small effect on the acquisition. Under mild regularity conditions we can formalize this intuition by bounding the partial derivatives of the acquisition with respect to each coordinate.

Fix a round t and consider acquisition α_t and optimizer \mathbf{x}_t^* . Let $S_t^0 := \{j : x_{t,j}^* \neq x_j^{\text{def}}\}$ be the set of components where \mathbf{x}_t^* differs from the default. For any set of components $S \subseteq S_t^0$, define

$$R_S(\mathbf{x}_t^*) := P_{S_t^0 \setminus S}(\mathbf{x}_t^*),$$

that is, $R_S(\mathbf{x}_t^*)$ is the configuration obtained from \mathbf{x}_t^* by *resetting* the components in S to their default values and keeping all the others as in \mathbf{x}_t^* . Equivalently, $R_S(\mathbf{x}_t^*)$ corresponds to precisely pruning the components of S .

Let $\Delta_t(\mathbf{x}) = \alpha_t(\mathbf{x}_t^*) - \alpha_t(\mathbf{x})$ denote the acquisition gap at round t .

Assumption A.3 (Per-component acquisition gaps, toy model). For each $j \in S_t^0$ there exists $\Delta_{t,j} \geq 0$ such that the acquisition gap when only component j is reset satisfies

$$\Delta_t(R_{\{j\}}(\mathbf{x}_t^*)) \geq \Delta_{t,j}.$$

Moreover, we assume a simple superadditivity property of the gap function (i.e., the joint gap is at least the sum of individual gaps; equivalently, no positive interaction effects between coordinates):

$$\Delta_t(R_S(\mathbf{x}_t^*)) = \alpha_t(\mathbf{x}_t^*) - \alpha_t(R_S(\mathbf{x}_t^*)) \geq \sum_{j \in S} \Delta_{t,j}, \quad \forall S \subseteq S_t^0.$$

Assumption A.3 says that each component has an associated ‘‘individual gap’’ $\Delta_{t,j}$, and that the combined effect of resetting a set of components is at least the sum of their individual gaps. This rules out positive interaction effects in which resetting two components together could be cheaper than resetting them separately, and is best viewed as a simplified model for intuition rather than a realistic assumption in complex BO problems.

Let $S_t^{\text{prune}} \subseteq S_t^0$ denote the set of components that BONSAI resets to default at round t , so that $\tilde{\mathbf{x}}_t = R_{S_t^{\text{prune}}}(\mathbf{x}_t^*)$.

Proposition A.4 (Thresholds constrain how many high-impact components can be pruned). *Suppose Assumption A.3 holds at round t , and that the BONSAI applies the relative gap rule so that $\Delta_t(\tilde{\mathbf{x}}_t) \leq \rho_t \tilde{\alpha}_t(\mathbf{x}_t^*)$. Then*

$$\sum_{j \in S_t^{\text{prune}}} \Delta_{t,j} \leq \rho_t \tilde{\alpha}_t(\mathbf{x}_t^*).$$

In particular, if $\Delta_{t,j} \geq \Delta_{\min} > 0$ for all $j \in S_t^{\text{prune}}$, then

$$|S_t^{\text{prune}}| \leq \frac{\rho_t \tilde{\alpha}_t(\mathbf{x}_t^*)}{\Delta_{\min}}.$$

Proof. By construction, $\tilde{\mathbf{x}}_t$ is obtained from \mathbf{x}_t^* by resetting the components in S_t^{prune} to their default values, that is, $\tilde{\mathbf{x}}_t = R_{S_t^{\text{prune}}}(\mathbf{x}_t^*)$. Applying Assumption A.3 with $S = S_t^{\text{prune}}$ yields

$$\Delta_t(\tilde{\mathbf{x}}_t) = \Delta_t(R_{S_t^{\text{prune}}}(\mathbf{x}_t^*)) \geq \sum_{j \in S_t^{\text{prune}}} \Delta_{t,j}.$$

The relative gap rule implies $\Delta_t(\tilde{\mathbf{x}}_t) \leq \rho_t \tilde{\alpha}_t(\mathbf{x}_t^*)$. Letting $\tau_t := \rho_t \tilde{\alpha}_t(\mathbf{x}_t^*)$ denote the (per-round) absolute threshold, we obtain

$$\sum_{j \in S_t^{\text{prune}}} \Delta_{t,j} \leq \tau_t.$$

If each $\Delta_{t,j} \geq \Delta_{\min}$, then

$$|S_t^{\text{prune}}| \Delta_{\min} \leq \sum_{j \in S_t^{\text{prune}}} \Delta_{t,j} \leq \rho_t \tilde{\alpha}_t(\mathbf{x}_t^*),$$

which proves the claimed bound. \square

Lemma A.5 (Coordinate sensitivity for ARD kernels). *Let α_t be the GP-UCB acquisition at round t with an ARD kernel of the form*

$$k(\mathbf{x}, \mathbf{x}') = \sigma_f^2 \phi \left(\sqrt{\sum_{j=1}^d \frac{(x_j - x'_j)^2}{\ell_j^2}} \right),$$

on a compact domain \mathbb{X} . Suppose ϕ is differentiable with $\phi'(r)$ bounded on $[0, \infty)$ (so that, in particular, the partial derivatives $|\partial k(\mathbf{x}, \mathbf{x}')/\partial x_j|$ are bounded on $\mathbb{X} \times \mathbb{X}$ for every j). Then there exists a constant $C_t < \infty$ (depending on the data, kernel hyperparameters, and β_t , but not on j) such that for all $\mathbf{x} \in \mathbb{X}$ and all $j \in \{1, \dots, d\}$,

$$\left| \frac{\partial \alpha_t(\mathbf{x})}{\partial x_j} \right| \leq \frac{C_t}{\ell_j}.$$

Proof. We sketch the argument. Differentiating the kernel with respect to the radial distance r gives

$$\frac{\partial k(\mathbf{x}, \mathbf{x}')}{\partial x_j} = \sigma_f^2 \phi'(r) \frac{\partial r}{\partial x_j}, \quad r = \sqrt{\sum_{m=1}^d \frac{(x_m - x'_m)^2}{\ell_m^2}}.$$

By the chain rule, for $r > 0$,

$$\left| \frac{\partial r}{\partial x_j} \right| = \frac{1}{r} \left| \frac{x_j - x'_j}{\ell_j^2} \right| \leq \frac{1}{r} \cdot \frac{|x_j - x'_j|/\ell_j}{\ell_j} \leq \frac{1}{\ell_j},$$

using $|x_j - x'_j|/\ell_j \leq r$. Hence $|\partial k(\mathbf{x}, \mathbf{x}')/\partial x_j| = \sigma_f^2 |\phi'(r)| \cdot |\partial r/\partial x_j| \leq \sigma_f^2 |\phi'(r)|/\ell_j$. By the lemma's hypothesis, ϕ' is bounded on $[0, \infty)$, so the partial derivative of the kernel is uniformly bounded by C'_k/ℓ_j for some finite constant C'_k independent of j . The bound extends continuously to $r = 0$ since the right-hand side is finite.

The GP posterior mean and variance are linear and quadratic forms in the kernel evaluations, respectively, with coefficients determined by the training data and the noise level. Differentiating those expressions with respect to x_j and applying the bound on $\partial k/\partial x_j$ shows that both $\partial \mu_{t-1}(\mathbf{x})/\partial x_j$ and $\partial \sigma_{t-1}(\mathbf{x})/\partial x_j$ are bounded in magnitude by C'_t/ℓ_j for some constant C'_t that depends on the data and hyperparameters but not on j . Since $\alpha_t(\mathbf{x}) = \mu_{t-1}(\mathbf{x}) + \beta_t \sigma_{t-1}(\mathbf{x})$, matching the GP-UCB definition in Section 2, we obtain the claimed bound with C_t proportional to $C'_t(1 + \beta_t)$. \square

Remark A.6 (Mixed continuous–discrete domains). Lemma A.5 assumes a continuous domain $\mathbb{X} \subset \mathbb{R}^d$ and uses the gradient $\partial\alpha_t/\partial x_j$ to bound coordinate sensitivity. Several of our experimental benchmarks (Joint NAS/HPO, Cell Network) include discrete coordinates, where this gradient bound does not apply directly. However, the BONSAI algorithm itself is gradient-free: it only evaluates the acquisition gap of single-coordinate resets and prunes whenever the gap is below the threshold (Algorithm 1). The sparsity-recovery guarantee under perfect ARD lengthscales separation (Theorem A.9) extends to discrete coordinates whenever the GP marginalizes irrelevant discrete coordinates exactly (i.e., the predictive distribution does not depend on those coordinates), in which case any reset of an irrelevant discrete coordinate produces zero acquisition gap. Lemma A.5 should be read as motivating—in the continuous case—why ARD lengthscales control which coordinates BONSAI tends to prune; the algorithm and its empirical behavior do not depend on this gradient bound.

Define the per-coordinate deviation $R_{t,j} := |x_{t,j}^* - x_j^{\text{def}}|$ at round t (so $R_{t,j} = 0$ for $j \notin A(\mathbf{x}_t^*)$). Lemma A.5 then implies that changing component j by $R_{t,j}$ can change the acquisition by at most $w_{t,j} := \frac{C_t R_{t,j}}{\ell_j}$, for some finite constant C_t that depends on the data, kernel hyperparameters, and β_t but not on j .

Now let $S \subseteq \{1, \dots, d\}$ be a set of components that we reset to their default values, and consider the candidate $\mathbf{x}' = R_S(\mathbf{x}_t^*)$, obtained by starting from \mathbf{x}_t^* and reverting the components in S back to \mathbf{x}^{def} . Resetting those components one at a time and summing the resulting changes in α_t yields the following bound on the acquisition gap:

$$\Delta_t(\mathbf{x}') = \alpha_t(\mathbf{x}_t^*) - \alpha_t(\mathbf{x}') \leq \sum_{j \in S} w_{t,j} = \sum_{j \in S} \frac{C_t R_{t,j}}{\ell_j}.$$

Under the relative gap rule with threshold ρ_t , any subset S satisfying $\sum_{j \in S} \frac{C_t R_{t,j}}{\ell_j} \leq \rho_t \tilde{\alpha}_t(\mathbf{x}_t^*)$ can therefore be reset to default while still respecting the relative constraint $\Delta_t(\tilde{\mathbf{x}}) \leq \rho_t \tilde{\alpha}_t(\mathbf{x}_t^*)$. In other words, $\rho_t \tilde{\alpha}_t(\mathbf{x}_t^*)$ acts as a per-round budget in the geometry induced by the ARD kernel: components with large lengthscales ℓ_j and small deviations $R_{t,j}$ incur little cost, while those with small ℓ_j and large $R_{t,j}$ can rapidly deplete the budget.

A.3 Sparsity Recovery Guarantees

While the regret bounds in Section 6 quantify the optimization cost of allowing acquisition gaps, a fundamental question remains: under what conditions is BONSAI guaranteed to recover the correct sparse structure of the objective? We establish formal sparsity recovery guarantees for BONSAI under two distinct structural scenarios: (1) exact learning of ARD lengthscales, and (2) additive acquisition functions.

Let $A_{\text{true}} \subset \{1, \dots, d\}$ denote the true active set of relevant parameters, such that the objective function $f(\mathbf{x})$ depends only on $\mathbf{x}_{A_{\text{true}}}$. Let $I_{\text{true}} = \{1, \dots, d\} \setminus A_{\text{true}}$ denote the strictly irrelevant parameters. The ideal pruning algorithm should ensure that for the returned configuration $\tilde{\mathbf{x}}_t$, the active set satisfies $A(\tilde{\mathbf{x}}_t) \subseteq A_{\text{true}}$, meaning all irrelevant parameters modified by the inner optimizer are successfully reverted to their defaults.

A.3.1 Scenario 1: Recovery via Perfect ARD Lengthscale Estimation

Our first result relies on the coordinate sensitivity of the GP surrogate with an ARD kernel. As established in Lemma A.5, the sensitivity of the GP-UCB acquisition function to a coordinate x_j is bounded by a term inversely proportional to its lengthscales ℓ_j . If the GP accurately identifies irrelevant dimensions, BONSAI is guaranteed to prune them. Importantly, this scenario assumes only that the GP hyperparameters are known—the same standard assumption used in GP-UCB regret bounds [Srinivas et al., 2010, Kim et al., 2025]—and does not require any additivity assumption on the acquisition function.

Assumption A.7 (Perfect Lengthscale Separation). The GP hyperparameter optimization successfully identifies the strictly irrelevant dimensions, such that for all $j \in I_{\text{true}}$, the learned ARD lengthscales $\ell_j = \infty$. For all relevant dimensions $j \in A_{\text{true}}$, the lengthscales are finite, $\ell_j < \infty$.

Assumption A.8 (Relevant Dimension Gap). Let $S_{\text{irrel}} = I_{\text{true}} \cap A(\mathbf{x}_t^*)$ be the set of irrelevant parameters modified by the acquisition maximizer \mathbf{x}_t^* . The threshold $\tau_t = \rho_t \tilde{\alpha}_t(\mathbf{x}_t^*)$ is chosen to be strictly smaller than the acquisition gap of reverting any single relevant parameter $j \in A_{\text{true}} \cap A(\mathbf{x}_t^*)$ alongside the irrelevant ones. Specifically, $\tau_t < \min_{j \in A_{\text{true}} \cap A(\mathbf{x}_t^*)} \Delta_t(R_{S_{\text{irrel}} \cup \{j\}}(\mathbf{x}_t^*))$.

Theorem A.9 (Exact Recovery under Perfect ARD). *Under Assumptions A.7 and A.8, applying BONSAI to the acquisition maximizer \mathbf{x}_t^* guarantees exact sparsity recovery with respect to the queried candidate: all irrelevant components are pruned, and no relevant components are pruned. That is, $A(\tilde{\mathbf{x}}_t) = A(\mathbf{x}_t^*) \cap A_{\text{true}}$.*

Proof. By Assumption A.7, for any $j \in I_{\text{true}}$, $\ell_j = \infty$. Following Lemma A.5, the partial derivative $\left| \frac{\partial \alpha_t(\mathbf{x})}{\partial x_j} \right| = 0$. Consequently, the acquisition function is perfectly flat along all dimensions $j \in I_{\text{true}}$. Resetting any subset of irrelevant components $S_{\text{irrel}} \subseteq I_{\text{true}}$ to their default values incurs zero loss in acquisition value: $\Delta_t(R_{S_{\text{irrel}}}(\mathbf{x}_t^*)) = 0$.

Because the relative threshold dictates $\tau_t \geq 0$, the pruned candidate $R_{S_{\text{irrel}}}(\mathbf{x}_t^*)$ is always strictly feasible under BONSAI's gap rule ($\Delta_t \leq \tau_t$). Moreover, since each irrelevant component contributes exactly zero to the acquisition gap, the greedy BONSAI procedure will prune them in any order without accumulating any gap. In this specific case of known lengthscales, the greedy algorithm therefore recovers the globally sparsest feasible configuration and will unconditionally prune all $j \in S_{\text{irrel}}$. (In the general case, the greedy procedure may not find the globally sparsest solution due to interactions between components; see Section 5.)

By Assumption A.8, pruning any additional relevant component $j \in A_{\text{true}}$ results in an acquisition gap strictly greater than τ_t , violating the threshold constraint. Therefore, BONSAI exactly recovers the true relevant components modified by the inner optimizer, yielding $A(\tilde{\mathbf{x}}_t) = A(\mathbf{x}_t^*) \setminus S_{\text{irrel}} = A(\mathbf{x}_t^*) \cap A_{\text{true}}$. \square

A.3.2 Scenario 2: Recovery under Additive Acquisition Models

While perfect lengthscale learning represents an asymptotic ideal, we can also prove sparsity recovery in finite-sample regimes if the acquisition function decomposes additively, formalizing the intuition from the additive model in Section A.2.

Assumption A.10 (Additive Acquisition). The acquisition function decomposes additively over coordinates: $\alpha_t(\mathbf{x}) = \sum_{j=1}^d \alpha_{t,j}(x_j)$. Consequently, the total acquisition gap for pruning a set of components $S \subseteq A(\mathbf{x}_t^*)$ (i.e., resetting those components to their defaults) is exactly $\Delta_t(R_S(\mathbf{x}_t^*)) = \sum_{j \in S} \Delta_{t,j}$, where $\Delta_{t,j} = \alpha_{t,j}(x_{t,j}^*) - \alpha_{t,j}(x_j^{\text{def}})$.

Remark: While standard acquisition functions like Expected Improvement (EI) are not strictly additive due to non-linear transformations, Assumption A.10 holds exactly for Additive UCB formulations [e.g., Kandasamy et al., 2015] designed for high-dimensional spaces, as well as for posterior samples utilized in Thompson Sampling under Additive GPs. For standard acquisition functions, this assumption serves as a localized, first-order Taylor approximation of the acquisition landscape near the optimum, consistent with the simplified model in Section A.2.

Assumption A.11 (Gap Separation). There is a strict separation in the per-component acquisition gaps between relevant and irrelevant parameters. There exist bounds $\epsilon \geq 0$ and $\Delta_{\text{min}} > 0$ such that:

- For all $j \in I_{\text{true}} \cap A(\mathbf{x}_t^*)$, $\Delta_{t,j} \leq \epsilon$ (irrelevant variables have minimal acquisition gaps).
- For all $j \in A_{\text{true}} \cap A(\mathbf{x}_t^*)$, $\Delta_{t,j} \geq \Delta_{\text{min}}$ (relevant variables have significant acquisition gaps).

Theorem A.12 (Sparsity Recovery under Gap Separation). *Under Assumptions A.10 and A.11, if the BONSAI threshold parameter ρ_t is chosen such that the absolute tolerance $\tau_t = \rho_t \tilde{\alpha}_t(\mathbf{x}_t^*)$ satisfies:*

$$|I_{\text{true}}| \epsilon \leq \tau_t < \Delta_{\text{min}}$$

then the sequential greedy BONSAI procedure (Algorithm 1) perfectly recovers the relevant structure: $A(\tilde{\mathbf{x}}_t) = A(\mathbf{x}_t^) \cap A_{\text{true}}$.*

Proof. By Assumption A.10, the total acquisition gap for pruning all modified irrelevant variables simultaneously is $\sum_{j \in I_{\text{true}} \cap A(\mathbf{x}_t^*)} \Delta_{t,j} \leq |I_{\text{true}}| \epsilon$. Because we require $\tau_t \geq |I_{\text{true}}| \epsilon$, the state where all irrelevant variables are reset to their default values is strictly feasible.

The sequential greedy algorithm operates by iteratively resetting the component that yields the smallest feasible gap. Because individual irrelevant components have gaps bounded by $\epsilon \leq |I_{\text{true}}| \epsilon \leq \tau_t$, the algorithm will iteratively successfully prune them.

Conversely, to prune even a single relevant variable $k \in A_{\text{true}}$, the candidate must incur an additional gap of at least Δ_{min} . Because the threshold dictates $\tau_t < \Delta_{\text{min}}$, no relevant variable can ever be pruned without violating the threshold constraint, regardless of the sequence of prior resets. Thus, the algorithm halts exactly when all $j \in I_{\text{true}} \cap A(\mathbf{x}_t^*)$ have been pruned, isolating the true sparse structure. \square

B BONSAI Algorithm

Incremental acquisition functions. To make the relative threshold ρ_t well-posed and comparable across acquisitions, we apply it to an *incremental* acquisition value above a baseline. Following Kim et al. [2025], we assume non-negative acquisition functions (any acquisition can be shifted by a constant to achieve this without changing the maximizer), so that $\alpha_t^* > 0$. We subtract the maximum *current* acquisition value across previously evaluated designs from the acquisition function: $\tilde{\alpha}_t(\mathbf{x}) = \alpha_t(\mathbf{x}) - b_t$, where $b_t = \max_{\mathbf{x} \in \mathcal{D}_{t-1}} \alpha_t(\mathbf{x}) \geq 0$ and \mathcal{D}_{t-1} denotes the set of designs evaluated before round t , before applying the relative rule.⁴ For log-acquisition functions [Ament et al., 2023], we apply BONSAI to exponentiated acquisition values (undoing the log transform) before forming b_t and applying the relative rule: $\Delta(P_S(\mathbf{x}^*)) \leq \rho \tilde{\alpha}(\mathbf{x}^*)$ with $0 \leq \rho < 1$. Equivalently, letting S range over subsets of $A(\mathbf{x}^*)$, $\tilde{\mathbf{x}} = P_{S^*}(\mathbf{x}^*)$ where $S^* \in \arg \min_{S \subseteq A(\mathbf{x}^*)} \{|S| : \Delta(P_S(\mathbf{x}^*)) \leq \rho \tilde{\alpha}(\mathbf{x}^*)\}$.

⁴We assume there are always previously evaluated designs (e.g., a space-filling initialization), so $\mathcal{D}_{t-1} \neq \emptyset$ for all $t \geq 1$.

Algorithm 1 BONSAI (sequential pruning with gaps)

```
1: Inputs: Acquisition functions  $(\alpha_t)_{t=1}^T$ , default  $\mathbf{x}^{\text{def}}$ , relative thresholds  $(\rho_t)_{t=1}^T$ 
2: for  $t = 1$  to  $T$  do
3:    $\mathbf{x}_t^* \approx \arg \max_{\mathbf{x} \in \mathbb{X}} \alpha_t(\mathbf{x})$ 
4:    $\tilde{\mathbf{x}}_t \leftarrow \mathbf{x}_t^*$ 
5:    $\mathcal{D} \leftarrow \{j : x_{t,j}^* \neq x_j^{\text{def}}\}$ 
6:    $b_t \leftarrow \max_{\mathbf{x} \in \mathcal{D}_{t-1}} \alpha_t(\mathbf{x})$  ( $\mathcal{D}_{t-1}$  is the set of previously evaluated designs, which is non-
   empty by Footnote 4)
7:   Define  $\tilde{\alpha}_t(\mathbf{x}) \leftarrow \alpha_t(\mathbf{x}) - b_t$ 
8:   Define  $\Delta_t(\mathbf{x}) \leftarrow \alpha_t(\mathbf{x}_t^*) - \alpha_t(\mathbf{x})$ 
9:   while  $\mathcal{D} \neq \emptyset$  do
10:     $\text{gap}_{\text{best}} \leftarrow +\infty, j_{\text{best}} \leftarrow -1$ 
11:    for  $j \in \mathcal{D}$  do
12:      Let  $\mathbf{x}' \leftarrow \tilde{\mathbf{x}}_t$  with component  $j$  reset to  $x_j^{\text{def}}$ 
13:       $g_j \leftarrow \Delta_t(\mathbf{x}')$ 
14:       $\text{feasible} \leftarrow (g_j \leq \rho_t \tilde{\alpha}_t(\mathbf{x}_t^*))$ 
15:      if  $\text{feasible}$  and  $g_j < \text{gap}_{\text{best}}$  then
16:         $\text{gap}_{\text{best}} \leftarrow g_j$ 
17:         $j_{\text{best}} \leftarrow j$ 
18:      end if
19:    end for
20:    if  $j_{\text{best}} \neq -1$  then
21:      Reset component  $j_{\text{best}}$  in  $\tilde{\mathbf{x}}_t$  to  $x_{j_{\text{best}}}^{\text{def}}$ 
22:       $\mathcal{D} \leftarrow \mathcal{D} \setminus \{j_{\text{best}}\}$ 
23:    else
24:      break
25:    end if
26:  end while
27:  Evaluate  $y_t = f(\tilde{\mathbf{x}}_t) + \varepsilon_t$ 
28:  Update the surrogate with  $(\tilde{\mathbf{x}}_t, y_t)$ 
29: end for
```

C Additional Empirical Evaluation and Experiment details

C.1 Minimal-Intervention Marker for Multi-Objective Problems

For multi-objective problems, the per-replication minimal-intervention marker overlaid in the bottom row of Figures 2–3 uses a hypervolume-based analog of the relative ϵ -constraint from Section 4. For each replication and each sparsity level k , let HV_k denote the hypervolume of the Pareto frontier formed by all explored points with at most k active dimensions, let $\text{HV}^* = \max_k \text{HV}_k$, and let HV^{def} be the hypervolume of $\{\mathbf{x}^{\text{def}}\}$. The marker is the smallest k for which $\text{HV}_k \geq \text{HV}^* - \epsilon(\text{HV}^* - \text{HV}^{\text{def}})$ at $\epsilon = 0.2$ (or the best-HV sparsity level if none qualifies).

C.2 Sequential Optimization Generation Times

As shown in Table 2, we find BONSAI has sequential generation times comparable to Standard BO and is significantly faster than the other default-aware methods, IR and ER.

Per-problem wall-time notes. SEBO is omitted from Optical Design in the batch ($q = 5$) setting (Table 4) since a single replication did not finish within a 4-day wall-time budget, due to the cost of homotopy continuation. On Joint NAS/HPO (a mixed integer/continuous space), BONSAI’s reported generation time is slightly below Vanilla BO’s because pruning yields sparser data, which in practice accelerates downstream GP fits and acquisition optimization on the same problem (the post-acquisition pruning loop adds only a small constant overhead per outer iteration).

	IR- L_0	ER- L_0	SEBO	BONSAI EI
JOINT NAS/HPO (26D)	24.7x ($\pm 1.4x$)	26.9x ($\pm 1.2x$)	51.8x ($\pm 5.0x$)	0.8x ($\pm 0.0x$)
OPTICAL DESIGN (146D)	–	3.4x ($\pm 0.2x$)	2.6x ($\pm 0.2x$)	2.0x ($\pm 0.2x$)
LASSODNA (180D)	3.7x ($\pm 0.1x$)	5.2x ($\pm 0.1x$)	3.3x ($\pm 0.3x$)	3.0x ($\pm 0.2x$)
CELL NETWORK (30D)	–	25.2x ($\pm 1.0x$)	95.3x ($\pm 6.8x$)	1.1x ($\pm 0.1x$)
BRANIN 50D (2D)	2.9x ($\pm 0.4x$)	3.0x ($\pm 0.3x$)	3.9x ($\pm 0.4x$)	1.0x ($\pm 0.1x$)
HARTMANN 50D (6D)	3.0x ($\pm 0.1x$)	5.5x ($\pm 0.4x$)	8.3x ($\pm 0.8x$)	1.5x ($\pm 0.1x$)
PRESSUREVESSEL 50D (4D)	2.3x ($\pm 0.3x$)	3.0x ($\pm 0.1x$)	2.1x ($\pm 0.3x$)	1.5x ($\pm 0.1x$)
DTLZ2 50D (6D)	–	3.9x ($\pm 0.1x$)	3.9x ($\pm 0.3x$)	1.4x ($\pm 0.1x$)

Table 2: Generation time relative to Vanilla BO (± 2 standard errors). The fastest default-aware method is shown in bold.

Active-dimension tolerance for continuous-relaxation baselines. For continuous baselines (IR, ER, SEBO), which optimize continuous relaxations and rarely return values exactly equal to the default, we count a coordinate as “inactive” for sparsity reporting if $|x_j - x_j^{\text{def}}| < 10^{-3}$ in normalized $[0, 1]^d$ coordinates.

C.3 Method Details

For mixed search spaces (Cell Network and Joint NAS/HPO), we use Ax’s default dispatch to optimize the acquisition function using the mixed-alternating optimizer, which interleaves local search on the discrete parameters with L-BFGS-B steps on the continuous parameters [Olson et al., 2025] for all methods. The mixed-alternating optimizer makes IR and ER very slow as shown in the wall times on problems with discrete parameters (Cell Network and Joint NAS/HPO).

Priors on the GP hyperparameters are given in Appendix D.

For IR and ER, we use 30 steps in homotopy continuation, with $a_{\text{start}} = 0.2$ and $a_{\text{end}} = 10^{-3}$, which follows the recommendation in Liu et al. [2023].

For constrained problems, if there is no feasible previously evaluated point, we optimize the probability of feasibility as the acquisition function (as in Olson et al. [2025]) and do not perform pruning or leverage IR/ER.

C.4 Problem Details

Synthetic Benchmarks. Each synthetic problem is embedded in a higher-dimensional search space by adding extra irrelevant parameters: Branin (2d), Hartmann (6d), PressureVessel (4d, 4 constraints) [Coello Coello and Mezura Montes, 2002], and DTLZ2 (6d, 2-objective) [Deb et al., 2002], all embedded in 50d spaces. Additional results on lower-dimensional benchmarks are provided below; these include *Branin 15d* (Branin’s 2d objective embedded in 15 dimensions), *Hartmann 15d* (Hartmann’s 6d objective embedded in 15 dimensions), and *BraninCurrin* (the standard 2d, 2-objective benchmark combining the Branin and Currin functions; not embedded), used in Appendix C.9 where exact pruning is computationally feasible.

Joint NAS/HPO is a real-world joint neural architecture search and hyperparameter optimization problem originating from a multi-task, multi-label neural network model at a large web services firm. The problem has 26 parameters that include the widths and depths of different blocks (integer parameters) and initial weights for layer norms (continuous parameters). Training and evaluating the model is computationally intensive, so sample efficiency is paramount. For this benchmark, we leverage a GP surrogate fitted to data collected from a real optimization run.

Optical Design is a real-world problem where the goal is to optimize 146 continuous parameters that control the surface morphology and geometry of optical components of a see-through display for augmented reality [Daulton et al., 2022]. The goal is to optimize two objectives: display efficiency and quality. Evaluating a design requires computationally intensive physical simulations; however, for the purposes of this benchmark, we leverage a neural network surrogate fit to real data collected from optimization runs.

LassoDNA [Šehić et al., 2022] involves tuning 180 parameters (each in $[-1, 1]$) corresponding to the penalty for each feature in a weighted Lasso regression to minimize MSE on the DNA dataset [Chang and Lin, 2011]. LassoDNA is available at github.com/ksehic/LassoBench, and the DNA dataset is available under a BSD-3-Clause license via LIBSVM at github.com/cjlin1/libsvm.

Cell Network is a 30d optimization problem [Dreifuerst et al., 2021] where the goal is to optimize the transmission power (an integer in $\{0, \dots, 10\}$) and downtilt (a continuous parameter in $[30, 50]$) for each of 15 antennas in a cellular network to minimize two objectives: under-coverage and over-coverage.

C.5 Reference Points for MOO

For the OpticalDesign problem, we follow Daulton et al. [2022]: we scale each objective by the corresponding component of the original reference point so that the transformed reference point is $(1, 1)$.

For CellNetwork, we use $[0.35, 0.35]$ as the reference point.

For the real-world MOO Ranking (10d) problem, we use $[0.0, 0.0]$ as the reference point in normalized objective coordinates (objectives are negated for maximization and shifted so the default \mathbf{x}^{def} outcome is non-negative).

For synthetic problems, we use default reference points for each in BoTorch [Balandat et al., 2020], which are commonly used in multi-objective Bayesian optimization papers [Daulton et al., 2020, 2021, 2023].

C.5.1 Real-world Ranking Problem

MOO Ranking is a value modeling tuning problem from a major web service, where there are 10 continuous parameters, and the goal is to learn the Pareto frontier between 2 engagement metrics. Again, we leverage a GP surrogate fit to data from real A/B tests [Feng et al., 2025].

Results The results for sequential optimization are shown in Figure 5. BONSAI finds near optimal solutions, with significantly fewer active dimensions than alternative methods. It is also significantly faster than IR and ER, as shown in Table 3.

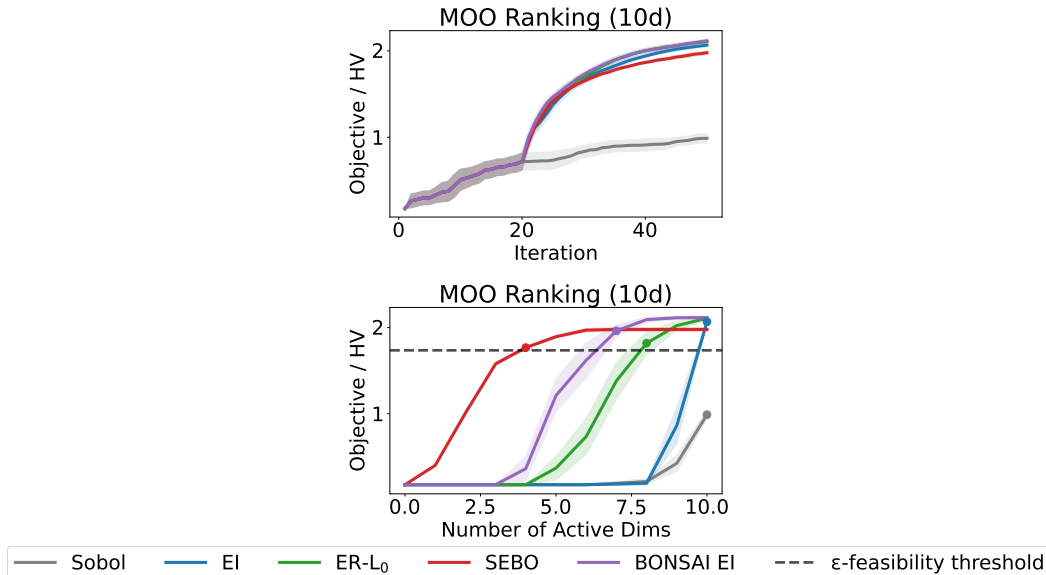


Figure 5: Real-world Ranking Problem. Top row: Objective or HV. Bottom row: Best Objective (or HV) value for each level of active dimensions. For MOO, the HV at sparsity level k is the hypervolume of the feasible Pareto frontier computed over all evaluated points with at most k active dimensions.

	IR- L_0	ER- L_0	SEBO	BONSAI EI
MOO RANKING (10D)	-	3.8x ($\pm 0.2x$)	5.6x ($\pm 0.4x$)	1.0x ($\pm 0.0x$)

Table 3: Generation time relative to Vanilla BO (± 2 standard errors). The fastest default-aware method is shown in bold.

C.6 Batch Optimization

We evaluate BONSAI in the batch setting where at each iteration, $q = 5$ points are generated. We find that BONSAI performs well in the batch setting too.

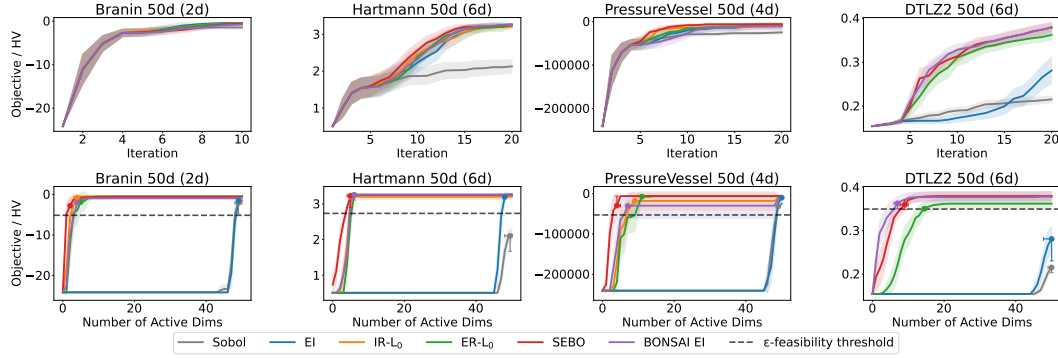


Figure 6: Optimization performance of BONSAI with batch optimization ($q = 5$) on synthetic problems. Top row: Objective or HV. Bottom row: Best Objective (or HV) value for each level of active dimensions. For MOO, the HV at sparsity level k is the hypervolume of the feasible Pareto frontier computed over all evaluated points with at most k active dimensions.

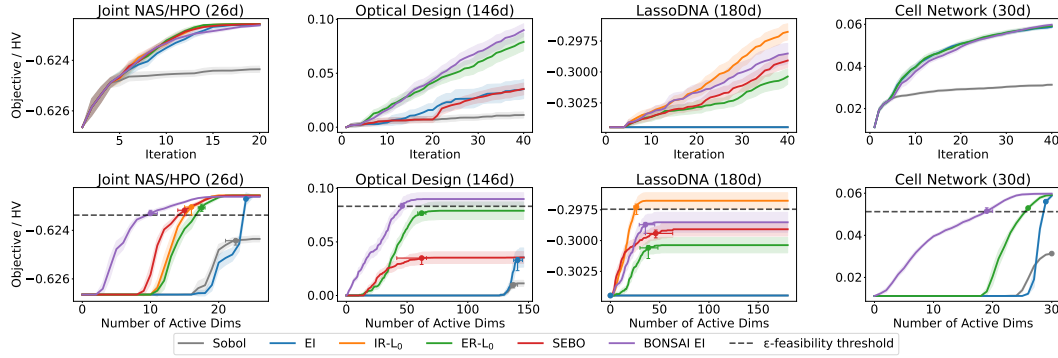


Figure 7: Optimization performance of BONSAI with batch optimization ($q = 5$) on real-world problems. Top row: Objective or HV. Bottom row: Best Objective (or HV) value for each level of active dimensions. For MOO, the HV at sparsity level k is the hypervolume of the feasible Pareto frontier computed over all evaluated points with at most k active dimensions.

	IR- L_0	ER- L_0	SEBO	BONSAI EI
JOINT NAS/HPO (26D)	27.3x ($\pm 0.8x$)	27.1x ($\pm 0.9x$)	78.0x ($\pm 5.3x$)	1.0x ($\pm 0.0x$)
OPTICAL DESIGN (146D)	–	3.4x ($\pm 0.2x$)	2.4x ($\pm 0.2x$)	2.7x ($\pm 0.2x$)
LISSODNA (180D)	2.9x ($\pm 0.1x$)	4.4x ($\pm 0.2x$)	5.3x ($\pm 0.5x$)	2.3x ($\pm 0.1x$)
CELL NETWORK (30D)	–	23.4x ($\pm 0.8x$)	–	1.0x ($\pm 0.0x$)
BRANIN 50D (2D)	3.0x ($\pm 0.2x$)	2.4x ($\pm 0.2x$)	8.3x ($\pm 1.2x$)	1.1x ($\pm 0.1x$)
HARTMANN 50D (6D)	3.2x ($\pm 0.1x$)	4.9x ($\pm 0.4x$)	17.1x ($\pm 1.6x$)	1.5x ($\pm 0.1x$)
PRESSUREVESSEL 50D (4D)	3.4x ($\pm 0.2x$)	3.4x ($\pm 0.2x$)	3.5x ($\pm 0.3x$)	1.4x ($\pm 0.1x$)
DTLZ2 50D (6D)	–	3.8x ($\pm 0.1x$)	10.9x ($\pm 1.2x$)	1.7x ($\pm 0.1x$)

Table 4: Generation time relative to Vanilla BO (± 2 standard errors). The fastest default-aware method is shown in bold.

C.7 BONSAI with UCB

We compare BONSAI (with qLogNEI) to BONSAI with UCB using a schedule on ρ_t proposed in Corollary A.2 with $c = 1$: $\rho_t = \frac{1}{t}$. We set the exploration parameter β_t in UCB to be $\beta_t = \sqrt{\log(t+2)}$ as in Kim et al. [2025]. To apply UCB to multi-objective problems, we use random hypervolume scalarizations [Zhang and Golovin, 2020], which reduce the multi-objective acquisition to a single-objective UCB at each iteration. Figures 8 and 9 show that UCB performs similarly to EI on most problems, but UCB performs worse on LassoDNA. Since EI acquisition functions (qLogNEI and qLogNEHVI) perform well across the board, we opt to use EI acquisition functions for the main-text experiments.

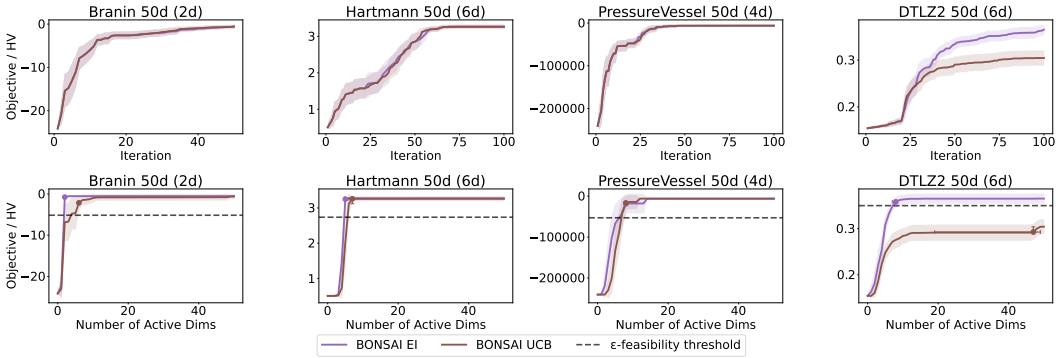


Figure 8: Comparison of BONSAI (with qLogNEI) to BONSAI with UCB on synthetic problems. Top row: Objective. Bottom row: Best Objective value for each level of active dimensions.

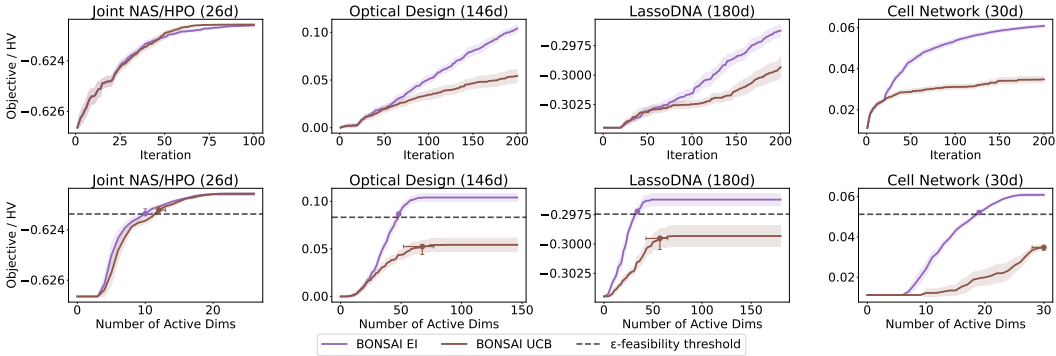


Figure 9: Comparison of BONSAI (with qLogNEI) to BONSAI with UCB on real-world problems. Top row: Objective. Bottom row: Best Objective value for each level of active dimensions.

C.8 Sensitivity with respect to ρ

We find that BONSAI is fairly robust with respect to the choice of ρ , as shown in Figures 10 and 11. We use $\rho = 0.2$ in the experiments in the main text.

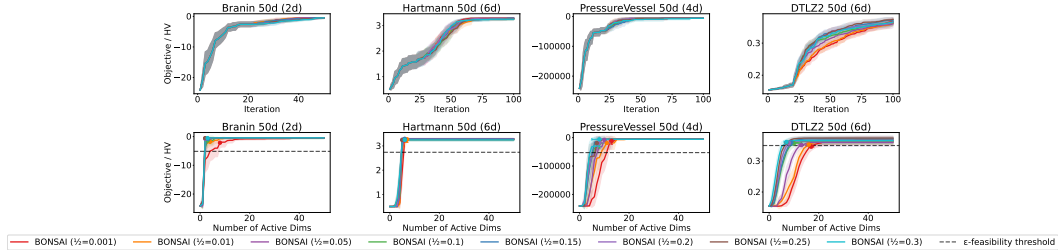


Figure 10: Top row: Objective or HV. Bottom row: Best Objective (or HV) value for each level of active dimensions. For MOO, the HV at sparsity level k is the hypervolume of the feasible Pareto frontier computed over all evaluated points with at most k active dimensions.

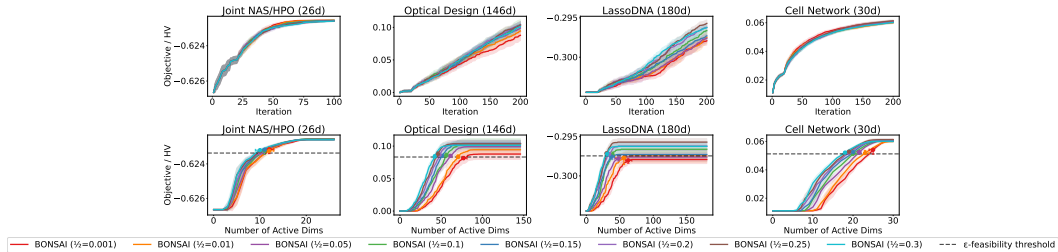


Figure 11: Top row: Objective or HV. Bottom row: Best Objective (or HV) value for each level of active dimensions. For MOO, the HV at sparsity level k is the hypervolume of the feasible Pareto frontier computed over all evaluated points with at most k active dimensions.

C.9 BONSAI with exact pruning

C.9.1 Low-dimensional benchmarks: all methods, with BONSAI exact pruning

In this section, we evaluate all methods (Sobol, Vanilla BO, IR, ER, SEBO, and BONSAI EI with both sequential greedy pruning and exact pruning) on the lower-dimensional benchmarks where exact pruning is computationally tractable. The full per-problem results in Figures 12 and 13 show that BONSAI is competitive with all default-aware baselines on these problems, and that BONSAI’s greedy and exact pruning variants yield comparable optimization performance and sparsity. Wall times relative to Vanilla BO for IR, ER, SEBO, BONSAI, and BONSAI Exact are reported in Table 5: as in the main experiments, BONSAI’s wall-time overhead is small while IR/ER/SEBO are substantially slower. Sequential greedy pruning is also significantly faster than exact pruning as dimensionality increases (e.g., on Hartmann 15d and Branin 15d), since exact pruning scales exponentially with dimensionality. Across all 7 problems (and replicates of each) considered in this section, BONSAI with exact and sequential greedy pruning yield the same first candidate 85.7% of the time after the Sobol initialization (we compare the first point after Sobol initialization since the models and acquisition functions are identical for the two pruning strategies at that point).

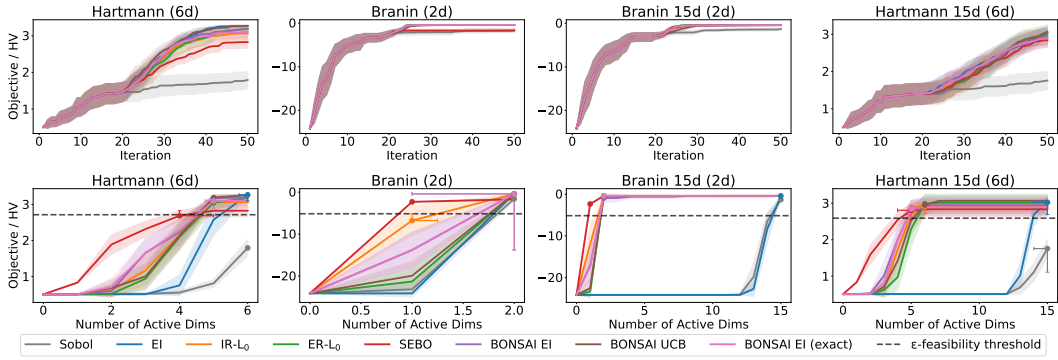


Figure 12: Optimization performance of BONSAl with exact and sequential greedy pruning with sequential optimization ($q = 1$). Top row: Objective or HV. Bottom row: Best Objective (or HV) value for each level of active dimensions. For MOO, the HV at sparsity level k is the hypervolume of the feasible Pareto frontier computed over all evaluated points with at most k active dimensions.

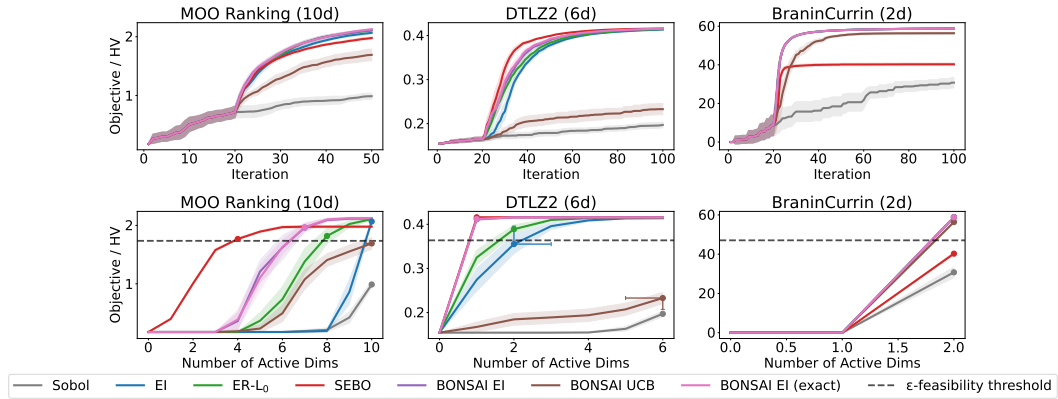


Figure 13: Optimization performance of BONSAl with exact and sequential greedy pruning with sequential optimization ($q = 1$). Top row: Objective or HV. Bottom row: Best Objective (or HV) value for each level of active dimensions. For MOO, the HV at sparsity level k is the hypervolume of the feasible Pareto frontier computed over all evaluated points with at most k active dimensions.

	IR- L_0	ER- L_0	SEBO	BONSAl EI	BONSAl EI (EXACT)
HARTMANN (6D)	3.5X ($\pm 0.2X$)	2.8X ($\pm 0.3X$)	7.0X ($\pm 0.8X$)	1.0X ($\pm 0.0X$)	1.0X ($\pm 0.1X$)
BRANIN (2D)	5.2X ($\pm 0.8X$)	5.4X ($\pm 0.5X$)	5.4X ($\pm 0.5X$)	1.0X ($\pm 0.2X$)	1.0X ($\pm 0.2X$)
MOO RANKING (10D)	–	3.8X ($\pm 0.2X$)	5.6X ($\pm 0.4X$)	1.0X ($\pm 0.0X$)	1.2X ($\pm 0.0X$)
DTLZ2 (6D)	–	5.6X ($\pm 0.1X$)	5.3X ($\pm 0.3X$)	1.1X ($\pm 0.0X$)	1.1X ($\pm 0.0X$)
BRANINCURRIN (2D)	–	5.4X ($\pm 0.2X$)	2.9X ($\pm 0.1X$)	1.0X ($\pm 0.1X$)	1.0X ($\pm 0.1X$)
BRANIN 15D (2D)	3.5X ($\pm 0.4X$)	3.2X ($\pm 0.4X$)	3.9X ($\pm 0.5X$)	1.0X ($\pm 0.1X$)	1.8X ($\pm 0.1X$)
HARTMANN 15D (6D)	3.7X ($\pm 0.1X$)	4.2X ($\pm 0.1X$)	6.7X ($\pm 0.9X$)	1.1X ($\pm 0.0X$)	2.0X ($\pm 0.0X$)

Table 5: Generation time relative to Vanilla BO (± 2 standard errors). The fastest default-aware method is shown in bold.

C.9.2 Low-dimensional benchmarks in the batch setting ($q = 5$)

We extend the all-methods comparison to the batch ($q = 5$) setting on the same low-dimensional benchmarks where exact pruning remains tractable (BraninCurrin, Branin 15d, Hartmann 15d, etc.); exact pruning remains infeasible on the higher-dimensional benchmarks of Section 7 since each batch element would require enumerating $O(2^{|A(\mathbf{x}_i^*)|})$ subsets. Figures 14 and 15 show that BONSAI remains competitive with the default-aware baselines in the batch setting, and that the two BONSAI pruning variants produce comparable optimization performance and sparsity, while sequential greedy pruning remains substantially faster.

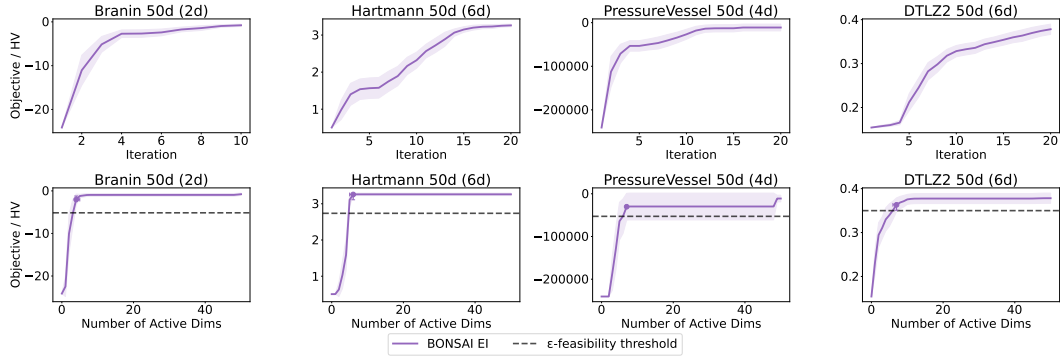


Figure 14: Optimization performance of BONSAI with exact and sequential greedy pruning with batch optimization ($q = 5$). Top row: Objective or HV. Bottom row: Best Objective (or HV) value for each level of active dimensions. For MOO, the HV at sparsity level k is the hypervolume of the feasible Pareto frontier computed over all evaluated points with at most k active dimensions.

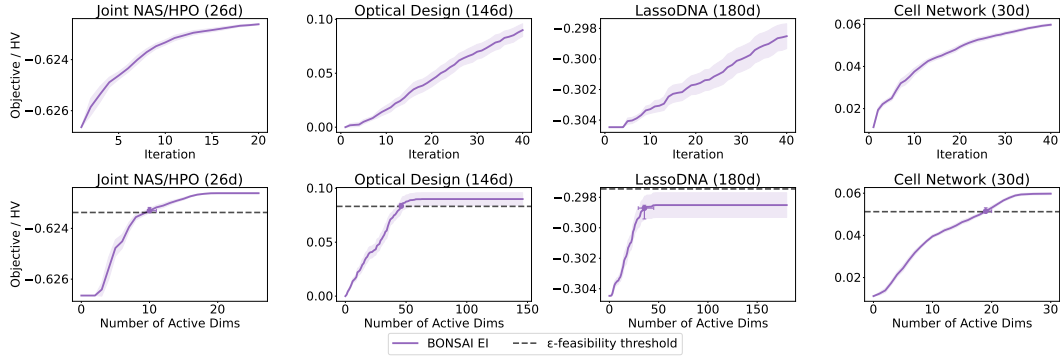


Figure 15: Optimization performance of BONSAI with exact and sequential greedy pruning with batch optimization ($q = 5$). Top row: Objective or HV. Bottom row: Best Objective (or HV) value for each level of active dimensions. For MOO, the HV at sparsity level k is the hypervolume of the feasible Pareto frontier computed over all evaluated points with at most k active dimensions.

	IR- L_0	ER- L_0	SEBO	BONSAI EI	BONSAI EI (EXACT)
HARTMANN (6D)	–	–	–	32.2 (± 1.2)	33.1 (± 1.2)
BRANIN (2D)	–	–	–	31.6 (± 5.3)	31.3 (± 5.2)
MOO RANKING (10D)	–	–	–	94.3 (± 2.6)	106.7 (± 3.7)
DTLZ2 (6D)	–	–	–	328.4 (± 9.9)	352.6 (± 20.2)
BRANINCURRIN (2D)	–	–	–	452.0 (± 32.9)	448.5 (± 31.2)
BRANIN 15D (2D)	–	–	–	52.5 (± 3.2)	95.7 (± 3.9)
HARTMANN 15D (6D)	–	–	–	44.4 (± 1.6)	82.4 (± 2.2)

Table 6: Average candidate generation time per iteration in seconds (± 2 standard errors). The fastest default-aware method is shown in bold.

C.10 Dimension Scaling Priors

All methods achieve less sparsity with dimension scaling priors [Hvarfner et al., 2024] than with MAP-SAAS. On problems with known numbers of active parameters, they do not find near-optimal solutions with the true number of active parameters. IR works slightly better than BONSAI on single-objective problems, but BONSAI performs best on the multi-objective problem (DTLZ2). Importantly, the optimization performance of BONSAI relative to Standard BO is unaffected by changing the model class; rather, the difference is just the level of sparsity achieved by default-aware methods.

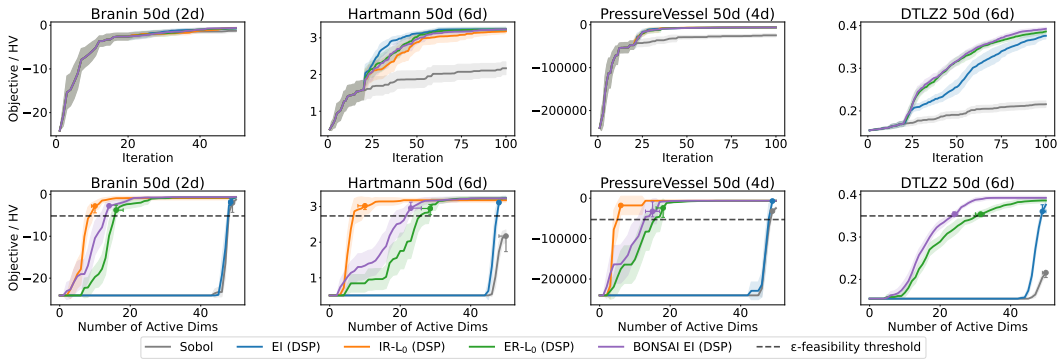


Figure 16: Sequential optimization performance of methods with a dimension-scaling prior (DSP). Top row: Objective or HV. Bottom row: Best Objective (or HV) value for each level of active dimensions. For MOO, the HV at sparsity level k is the hypervolume of the feasible Pareto frontier computed over all evaluated points with at most k active dimensions.

C.11 IR/ER Sensitivity Analysis

In our experiments, we set the penalty coefficient in IR and ER to be 0.01, which was a good default value from [Liu et al., 2023]. In addition, we test different values of the penalty coefficient on synthetic problems to analyze the sensitivity of IR and ER. This analysis validates that 0.01 is a reasonable choice.

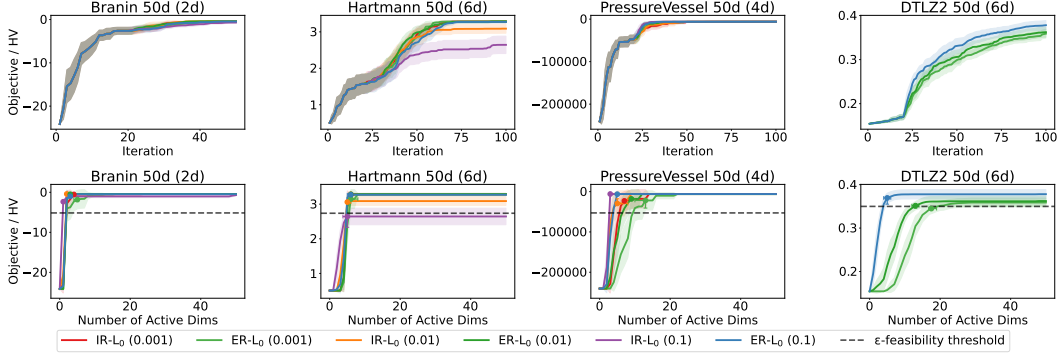


Figure 17: Top row: Objective or HV. Bottom row: Best Objective (or HV) value for each level of active dimensions. For MOO, the HV at sparsity level k is the hypervolume of the feasible Pareto frontier computed over all evaluated points with at most k active dimensions.

C.12 Improved Lengthscale Estimation

In this section we show that BONSAI improves the lengthscale estimation on the 6d DTLZ2 problem embedded in a 50d space. As illustrated in Figure 2, BONSAI outperforms Standard BO on this problem. Following [Hvarfner et al., 2025], we fit a GP with a dimension-scaling prior to the 100 trials collected by each replication of Sobol, Standard BO, and BONSAI. The distribution over replications of the log-lengthscales is illustrated in Figure 18.

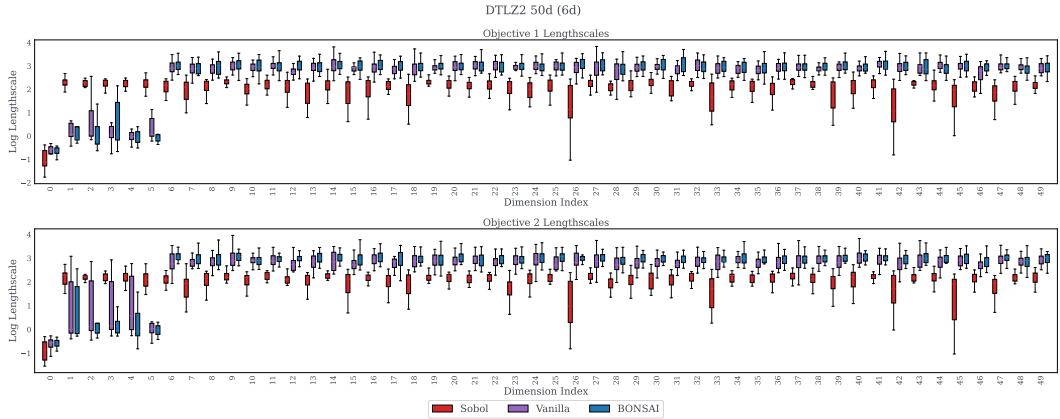


Figure 18: Estimated lengthscales using data collected by different methods on the DTLZ2 50d (6d) problem. Using the data collected by BONSAI consistently results in more accurate lengthscale estimation.

We observe that we are consistently able to identify the 6 non-redundant parameters when using the data collected by BONSAI. In comparison, using the data collected by Sobol and Standard BO results in sometimes failing to infer small lengthscales for the 6 non-redundant parameters, demonstrating that using pruning makes it easier for the underlying GP model to infer better lengthscales. We believe this is one of the reasons why BONSAI outperforms Standard BO on this problem.

D MAP Estimation of SAASBO (MAP-SAAS)

To improve scalability relative to fully Bayesian SAASBO, we use an ensemble MAP approximation in which a small number of global sparsity scales are sampled and the remaining GP hyperparameters are fit via MAP. The fitting procedure is described in Algorithm 2. This ensemble construction approximates posterior uncertainty over sparsity patterns while retaining the computational efficiency of MAP-based GP fitting. For each model in the ensemble, we use a Tophat($10^{-2}, 10^4$) prior over the signal variance s_m and a Gamma(0.9, 10.0) prior over the noise variance σ_m^2 .

Algorithm 2 Ensemble MAP-SAAS GP

Require: Training data $X \in \mathbb{R}^{n \times d}$, $Y \in \mathbb{R}^{n \times 1}$

Require: Ensemble size $M \leftarrow 4$

- 1: Sample $\tau_1, \dots, \tau_M \stackrel{\text{iid}}{\sim} \text{HalfCauchy}(0.1)$
 - 2: Form batched data $X^{(b)}, Y^{(b)} \in \mathbb{R}^{M \times n \times d}$
 - 3: **for** $m = 1$ **to** M **do**
 - 4: Define a Matérn-5/2 GP with ARD lengthscales $\ell_{m,1:d}$
 - 5: Use priors: $\ell_{m,j}^{-2} \sim \text{HalfCauchy}(\tau_m)$ (sparsity-inducing SAAS prior on the inverse squared lengthscales), $\sigma_m^2 \sim \text{Gamma}(0.9, 10.0)$, $s_m \sim \text{Tophat}(10^{-2}, 10^4)$
 - 6: Fit $\{\ell_{m,j}, \sigma_m^2, s_m\}$ by MAP
 - 7: **end for**
 - 8: Return a uniform Gaussian mixture posterior over ensemble members
-

Additionally, we compare BONSAI with MAP-SAAS to BONSAI with a GP with a dimension-scaling prior (DSP) [Hvarfner et al., 2024] and SAASBO [Eriksson and Jankowiak, 2021] and find that MAP-SAAS induces more sparsity.

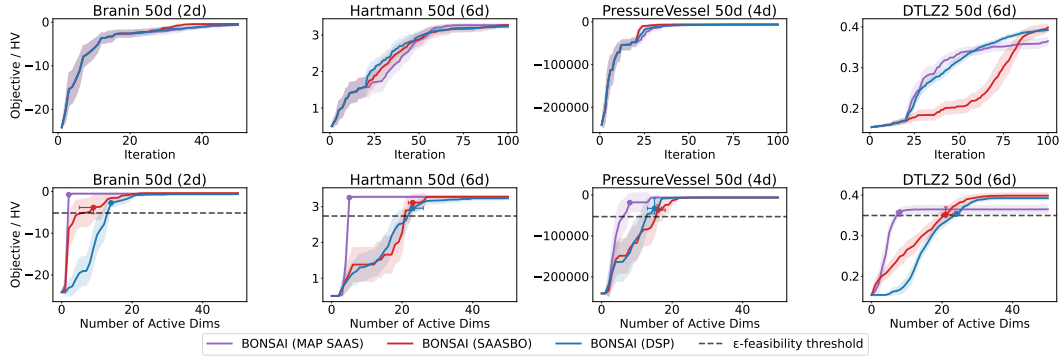


Figure 19: Sequential optimization performance of BONSAI with on synthetic problems with MAP-SAAS and the dimension-scaling prior. Top row: Objective or HV. Bottom row: Best Objective (or HV) value for each level of active dimensions. For MOO, the HV at sparsity level k is the hypervolume of the feasible Pareto frontier computed over all evaluated points with at most k active dimensions.

E Extensions of IR and ER

IR can be extended to constrained qLogNEI in a straightforward way, since IR changes the objective by adding a penalty term based on the ℓ_0 -norm. Similarly, ER can also be extended to constrained qLogNEI since the penalty in ER is simply added to the acquisition function externally.

Extending IR to multi-objective problems is non-trivial. For IR, one could penalize each objective by the sparsity penalty, but that would have a multiplicative effect on the hypervolume. Alternatively, one could subtract the sparsity penalty from the hypervolume of a set of points, but that would require extending the penalty to apply to sets of points. The issues of scale between hypervolume and the sparsity penalty may make it difficult to choose a reasonable value of the sparsity penalty coefficient.

For ER in the multi-objective setting, we apply the ℓ_0 penalty externally to qLogNEHVI: at each acquisition optimization, we compute $\alpha_t^{\text{ER}}(\mathbf{x}) = \text{qLogNEHVI}_t(\mathbf{x}) - \lambda \cdot \|\mathbf{x} - \mathbf{x}^{\text{def}}\|_0$, where the penalty coefficient λ is set to the same default value 0.01 used in single-objective ER. We apply the penalty after the log transform (i.e., directly to qLogNEHVI’s output rather than to the raw NEHVI), so that the penalty acts on the same scale as the log-acquisition. As in single-objective ER, we use 30 homotopy continuation steps with $a_{\text{start}} = 0.2$ and $a_{\text{end}} = 10^{-3}$ following the recommendation of Liu et al. [2023].

F Additional Related Work

Conservative and safe bandits with baselines. A related line of work studies *conservative* or *safe* policies that constrain performance relative to a baseline arm or configuration, e.g., by requiring the cumulative reward not to fall too far below a status-quo level [e.g., Kazerouni et al., 2017, Sui et al., 2015]. BONSAI is not a safety mechanism of this particular type: our constraint is imposed on the acquisition rather than on the unknown objective, and the primary goal is to simplify recommendations in input space rather than to provide outcome-level safety guarantees. We view these approaches as complementary, and BONSAI could be combined with conservative BO when both simplicity and outcome-level constraints are required.

Variable selection and shrinkage for high-dimensional BO. Other work exploits sparsity to improve BO in high dimensions. Methods such as SAASBO [Eriksson and Jankowiak, 2021] and VSBO [Shen and Kingsford, 2023] aim to identify a small set of influential dimensions via shrinkage priors on kernel lengthscales or forward-stage selection using importance scores. Hvarfner et al. [2024] propose a dimensionality-scaled hyperprior whose mean grows with \sqrt{d} , progressively shrinking lengthscales toward larger values as dimensionality increases. These techniques primarily target the structure of the objective f to improve sample efficiency. However, even when only a few dimensions are relevant, the recommended configuration can still deviate substantially from a practitioner-chosen default across many components. BONSAI instead measures complexity directly via the ℓ_0 distance to a user-specified default and prunes low-impact deviations regardless of whether they arise in globally relevant or irrelevant dimensions.

Explainable and interpretable BO. Recent work has begun to study the interpretability of BO recommendations. For example, Chakraborty et al. [2025] explain BO solutions by identifying tunable subspaces and quantifying parameter-wise contributions, and Adachi et al. [2024] explore techniques to make BO behavior more transparent to practitioners. BONSAI is complementary: rather than explaining a potentially complex recommendation in the full input space, it directly simplifies the recommendation by reverting as many components as possible to their default values while maintaining a near-optimal acquisition value. This can be useful both on its own and as a front-end to post-hoc explanation methods applied to the pruned suggestion.

Cost-aware and switching-cost Bayesian optimization. Several works incorporate explicit costs into BO. Cost-aware BO methods modify the acquisition to trade off reward and cost, or to preferentially query cheap configurations; see, e.g., work on cost-varying or subset-aware BO [Tay et al., 2023, Song et al., 2022]. Lin et al. [2021] consider modular black-box systems in which changing components incurs switching costs and optimize a cost-augmented objective. BONSAI differs from these approaches in two ways. First, it does not require specifying or learning a cost function over individual input parameters. Instead, it enforces a hard constraint on the *acquisition gap* relative to the maximizer and, within that constraint, explicitly prefers the candidate with the fewest deviations from a fixed default configuration. Second, BONSAI is implemented as a post-processing step, leaving the underlying surrogate and acquisition function unmodified, and can thus be straightforwardly applied across a broad range of settings.

Lengthscale-thresholding as a pruning baseline. A natural alternative to BONSAI would be to eliminate changes in dimensions whose estimated ARD lengthscale exceeds a threshold. However, this approach has important limitations: (1) it is not straightforward to apply in multi-output settings (multi-objective and constrained problems) where multiple GPs with different lengthscale estimates must be reconciled; and (2) choosing a lengthscale threshold is itself a sensitive hyperparameter—for constrained problems, a lengthscale that appears large for the objective GP may correspond to a dimension critical for constraint satisfaction. In contrast, BONSAI’s relative acquisition tolerance ρ has a natural interpretation across all problem types (single-objective, constrained, and multi-objective), and we demonstrate its robustness to the choice of ρ in Appendix C.8.

G Future Work

In this section, we discuss directions for future work.

BONSAI measures simplicity using coordinate-wise ℓ_0 distance to the default, which is appropriate when each coordinate corresponds to a semantically meaningful and independently actionable knob. When parameters are correlated or meaningful only as groups (common in systems tuning), a grouped or weighted sparsity notion can be more realistic; we view BONSAI as a first step toward such structured pruning. Empirically, we also compare against exact pruning, which can reset multiple knobs simultaneously in one-shot and is capable of group-level pruning, and we find similar performance to sequential greedy pruning (Appendix C.9).

There are several directions for future work. First, it would be useful to develop tighter sparsity guarantees that move beyond the simplified per-component perspective in Section A.2 and to better characterize when greedy pruning matches the combinatorial optimum. Second, extending the theoretical analysis to EI and additional acquisition functions would require new tools, since the current proof techniques rely on confidence bounds. Third, it would be interesting to integrate BONSAI with more sophisticated models of user or operator preferences, for example allowing different components to have different “weights” in the ℓ_0 cost or incorporating structured defaults (such as grouped parameters). Finally, combining BONSAI with post-hoc explanation methods may further improve the transparency of BO-driven decision-making in practice.